HIGH-THROUGHPUT PHOTOBIOREACTOR FOR MICROALGAL BIOFUEL ASSAY

An Undergraduate Research Scholars Thesis

by

EVAN RICHARDS, ALEX SHAMMAI, and NIDA WARSI

Submitted to the Undergraduate Research Scholars program
Texas A&M University
in partial fulfillment of the requirements for the designation as an

UNDERGRADUATE RESEARCH SCHOLAR

Approved by
Research Advisor: Dr. Arum Han

May 2016

Major: Electrical Engineering

TABLE OF CONTENTS

ABSTRACT

High-Throughput Photobioreactor for Microalgal Biofuel Assay

Evan Richards, Alex Shammai, and Nida Warsi
Department of Electrical and Computer Engineering
Texas A&M University

Research Advisor: Dr. Arum Han
Department of Electrical and Computer Engineering
Department of Biomedical Engineering

Microalgae are emerging as a source of future biofuel due to high oil productivity and low environmental impact. Optimizing microalgal growth and oil production by the study of growth conditions will address the high production cost of microalgal biofuel. A testing solution is needed for high-throughput studies. Here we present a photobioreactor (PBR) capable of providing control of multiple culture conditions to investigate their effect on microalgal growth. A light source was designed to implement light intensity, cycle, and wavelength control, and a feedback control system was designed to control temperature. Both subsystems are managed by a microcontroller. Microalgal cells were isolated and analyzed with an integrated droplet microfluidics platform at single cell resolution. The PBR has been successfully used to characterize *Chlamydomonas reinhardtii* species by various testing growth conditions in parallel.

ACKNOWLEDGMENT

This work was supported by the National Science Foundation (NSF), Emerging Frontiers in Research and Innovation (EFRI) grant #1240478, and NSF Research Experience and Mentoring (REM) grant #1519008.

This work was also supported by Texas A&M University's Engineering Innovation Center (EIC)

CHAPTER I

INTRODUCTION

Traditional fuel sources present ongoing problems including environmental concerns and finite oil reserve depletion [1]. New sources for carbon-neutral and sustainable energy production must be explored. Oil producing crops such as corn and soy can provide renewable biofuels, but they require competition with food supply and are challenging in large-scale production. Compared to these feedstocks, microalgae have higher productivity (faster growth rates, higher oil yield), low environmental impact, and less competition with land usage and food [2]. Although microalgae have a potential as a source of biofuels, the production cost is still not economically competitive, which requires significant improvements including the optimization of microalgal culture conditions and identifying high-performance microalgal strains.

Currently, developing microalgae as an energy source requires further optimizing culture conditions to enhance their growth and oil production. Microalgal growth and oil production are affected by culture conditions such as light intensity, light cycle, light wavelength, temperature, nutrient, pH, and CO_2 and oxygen exposure. Because the effects of culture conditions on microalgal growth and oil production are complex, a wide dataset is needed to study them. Conventionally, experiments on microalgae are mainly conducted in lab-scale flasks, open raceway ponds, or closed photobioreactors (PBR) [3]. Present testing systems are not fit to practically collect the wide dataset needed to study the relationships between culture conditions and microalgal growth due to their low throughput, large scale, and cost. A novel screening

platform is needed which controls culture conditions in parallel and provides a high-throughput screening.

Microfluidics and lab-on-a-chip technologies have been widely used in various biological applications due to their capabilities to precisely control, monitor and manipulate samples at the nano to picoliter scales [4]. A microfluidic platform provides the high-throughput assay capabilities needed to practically experiment with microalgae. Furthermore, microfluidic platforms offer portability due to their small form factor and low weight construction. This approach also offers a low-cost solution due to the reduced amount of material and space required [5].

Here, we present a high-throughput bilateral PBR assay that is capable of the throughput needed for efficient manipulation of culture factors and standardized testing. The PBR, a container for microfluidic devices, controls temperature, light intensity, cycle, and wavelength. Photobioreactors have been constructed, and their capability to control culture conditions has been tested. The results from culture experiments demonstrate the PBR's screening capability and the potential for use towards the goal of growth optimization to improve microalgal biofuels.

CHAPTER II

PHOTOBIOREACTOR AND MICROFLUIDIC SYSTEM

The photobioreactor

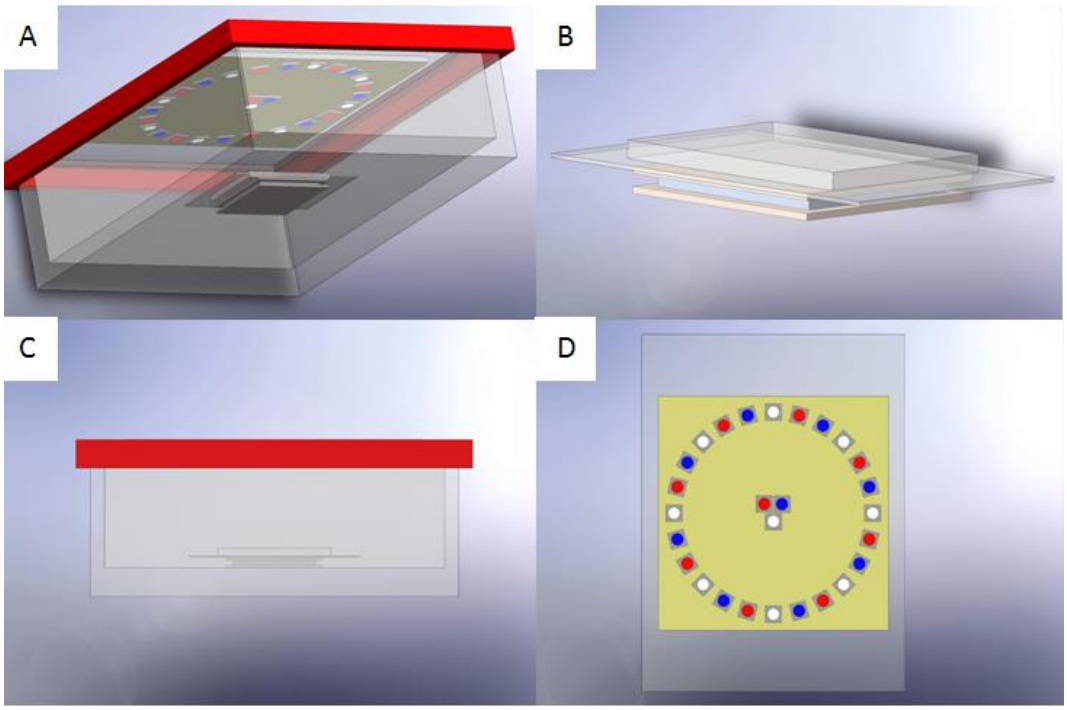

Figure 1. The experimental setup of the PBR container. A) The placement of the microfluidic device under the PCB. B) The microfluidic device bonded on the glass slide is above the heater. D) The light control PCB is embedded in the container lid.

The PBR shown in Figure 1, a closed system for each microfluidic device culture, controls temperature, light intensity, cycle, and wavelength. The external container (Pyrex) of each PBR includes a light source embedded in the top lid. The glass substrate of the microfluidic device is between the heater and a plastic dish for water containment. The plastic dish has a cut out to fit the device in its center. The dish holding the microfluidic device sits centered under the light source inside the container, and the container can be sealed to minimize water evaporation. The

lid includes a port to pass a thermocouple and power supply wires for the heating element that will be connected to a microcontroller. Two power supplies (Agilent 3630), the light and temperature control circuits, and microcontroller are located adjacent to the array of PBRs.

Motivation for microfluidics

Microfluidics provide the high-throughput assay capabilities needed to practically experiment with microalgae because of their capability to perform multiple cultures that begin from one cell on a single device. Additionally, microfluidic devices are rapidly fabricated, enabling easy variation of the experimental setup and device geometry. Proven by control system characterizations, the PBR system is expandable to control culture conditions of devices with other geometry or integrated systems. Other microfluidic applications include systems that enable functions such as transport, separation, and mixing [6]. Furthermore, microfluidic platforms offer portability due to their small form factor and low weight construction, which reduces the overall PBR setup size.

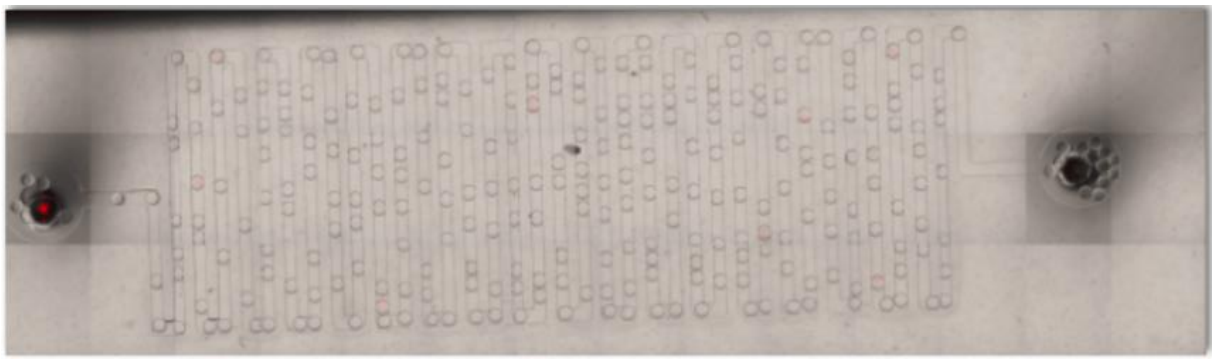

Figure 2. The combined bright field and autofluorescence image of the microfluidic device. The left and right ends of the channels are the inlet and outlet of the device.

The geometry of the two devices, shown in Figure 2, fabricated for each experiment consists of rows of channels used as a growth chamber for droplets. Polydimethylsiloxane (PDMS) is used as a resin to create microfluidic devices by a soft lithography process. In addition to its low cost, PDMS is chosen to fabricate microfluidic devices because it is transparent at optical frequencies, has a low autofluorescence, and is easy to mold [7]. The microfluidic fabrication procedure allows reuse of the master mold. Reuse of molds results in a shorter fabrication cycle, which is desirable for biological experiments where many devices may need to be created.

Microfluidic device method

The method that was used to fabricate microfluidic devices is divided into three main steps: preparing PDMS, PDMS bonding, and device preparation. First, PDMS is prepared by mixing a Sylgard 184 silicone base and curing agent using a 10:1 ratio. This mixture is degassed to remove bubbles and poured over a master mold created by 3D printing. The covered mold is then baked to cure the PDMS. After the curing time, the PDMS is easily cut and peeled from the mold. These preparation steps determine the properties of the cured PDMS. The ratio of the silicone base to curing agent, the curing time, and the curing temperature affect PDMS properties. Inlets and outlets to the channels were then made by puncturing the relatively flexible PDMS.

After the PDMS has been cured with the mold of microfluidic structures, it must be bonded to a glass substrate to create the bottom surface of the channels. PDMS is inherently hydrophobic with nonreactive surfaces. In this state, it is difficult to bond PDMS to the glass substrate. PDMS temporarily becomes hydrophilic and reactive when exposed to an oxygen plasma which allows

bonding with silicon, glass, or another PDMS piece [8]. The prepared PDMS was treated with oxygen plasma then immediately bonded onto a glass substrate.

Shortly after exposure to oxygen plasma, the PDMS is again hydrophobic. Aquapel is a fluorous polymer used to render glass surfaces hydrophobic [9]. The channels of the microfluidic device were treated with Aquapel by filling the channels with the solution and then flushing the channels with air. To prevent droplets merging a solution was prepared with 2 weight % 008-FluoroSurfactant (RAN Biotechnologies) in FC40 electronic liquid (Fluorinert). The channels were filled with the oil and surfactant solution then sealed. The entire device is then submersed in water for degassing in a vacuum chamber before culture preparation.

Microfluidic culture

Chlamydomonas reinhardtii were initially cultured under 80 μmol photon m^{-2} s^{-1} light intensity at 21ºC. *C. reinhardtii* were collected 2 days after each subculture for use in analysis. Small volumes of the previously cultured cell sample were emulsified in the oil and surfactant solution to create droplets containing microalgae cells by a droplet generation process. This droplet generation process is significant because the volume of each droplet determines the amount of Tris-Acetate-Phosphate (TAP) media available for the individual droplet cultures to grow [10]. In the growth analysis process, only droplets that contain 1 cell are tracked, so the cell concentration in the sample must be tuned. Before droplet generation, the culture media was refreshed, and the cell concentration was diluted using a hemocytometer to result in approximately 1 cell per droplet.

For our experiments, two 1 ml syringes filled with the cell sample and oil solution were inserted into two syringe pumps set to 150 μl/hr and 350 μl/hr, respectively. To avoid waiting for the excess air to be pushed through the system, the air bubbles from the syringes and the connected 150 μm diameter tubing were removed. This is significant because the cells in the media begin to settle over time, decreasing the concentration of cells in the prepared sample. Using the tubing, the two syringes were connected to the inlets of the droplet generator, and the outlet of the droplet generator was connected to the inlet of the culture device. The tubing from the outlet of the culture device was left in a reservoir to collect waste during the droplet generation process.

After the syringe pumps are turned on, the droplets are formed by a T-junction on the droplet generation device. The size of the droplets is partially dependent on the flow rate of the two incident fluids and the geometry of the channel intersection [11]. The width of the cell sample, oil solution, and outlet channels was 120 μm, 150 μm, and 160 μm, respectively. The target size of these droplets was 180-200 μm diameter.

After droplet generation, both bright field and chlorophyll autofluorescence images of all droplets were obtained using a Zeiss Axio Observer Z1 microscope (Carl Zeiss MicroImaging, LLC) equipped with a digital camera (Orca Flash2.8 CMOS Camera) and filter. The filter was set with an emission range of 500–550 nm and excitation range of 450–490 nm. These images were used as references (day 0) and subsequent images were taken every day after the culture began. The growth of *C. reinhardtii* was characterized by tracking the number of cells in individual droplets. A set number of droplets were analyzed for each of the light intensity, wavelength, or temperature experiments. The size of droplets was tracked using image analysis

software (Image J) to ensure evaporation or pressure did not cause a significant change in droplet size.

CHAPTER III

CONTROLLED MULTIWAVELENGTH LED LIGHT SOURCE

Motivation for improved light source

To create a PBR with a high level of control over light conditions while maintaining a portable form factor, an arrangement of overhead Light Emitting Diodes (LED) was used. An LED light source offers advantages compared to a standard, white tabletop desk lamp bulb used in the conventional testing setup shown in Figure 3. One of the shortcomings associated with this component is that the lab user could not easily vary the intensity of the light incident on the sample while retaining a reliable area of uniformity. To change the intensity of the light, the user must raise or lower the bulb over a light sensor to achieve a desired intensity, which can be cumbersome. Moreover, the area of the light's uniform distribution varies in size as the height of the bulb changes, meaning the lab user loses control over uniformity as well. For an efficient testing solution, the PBR should provide linear control over the intensity and consistent uniform area to the user. Another limitation of the previous setup was its inability to vary the wavelength of light. Previous studies on microalgae growth patterns have shown that red light (620 -720nm) and blue light (450 – 495nm) wavelengths can affect growth rates in various microalgae strains [12]. As such, it was necessary to include more wavelength options in a new testing setup. Although the old setup could use a simple timer to simulate a day and night situation, it could not provide high frequency light cycles that are now of interest in microalgae growth experiments [13]. Precise light cycle control was also an advantage the lab user should be provided. Furthermore, to gain the best possible understanding on how these conditions effected the growth

and oil production of microalgae, one should be able to control all of the previously mentioned functionalities simultaneously.

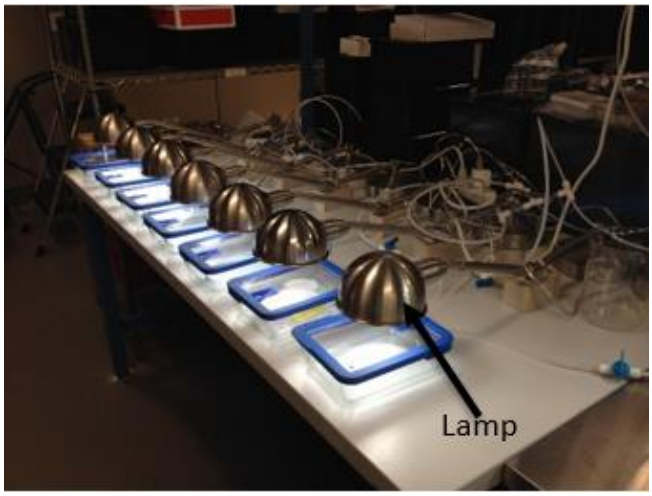

Figure 3. This is the conventional culture setup. An incandescent light bulb is used to provide light to microalgae

Considering other components and subsystems

One major consideration when designing the new light control component was that the light distribution on the sample needed to be uniform to have consistent exposure across all microalgae samples. The vertical distance away from the sample, the size of the microfluidic testing platform, and the pattern of the light emitters' arrangement are all parameters that determine light uniformity requirement in our closed system. Tidiness and simplicity of our final design were also important factors to consider in order to reduce cost of materials and to make future repeatability easy. For this reason, control of both the light and temperature circuits was consolidated by using an Arduino Uno microcontroller. The LED circuit was also designed to utilize a common lab bench power supply.

Design methods

White (Luxeon 3535L), Red (Luxeon Z Color LXZ1-PA01), and Blue (Luxeon Z Color LXZ1-PR01) LEDs were chosen because they could provide a wide range of intensity and small form factor. Due to the size of the surface mount package type, Printed Circuit Boards (PCB) were required for testing and prototyping.

LED array design

To prevent error in results, the light source should provide a uniform distribution of light over the area of cells being tested. To provide a uniform area of light, the arrangement of the LEDs were designed with irradiance interference in mind. During preliminary testing, LEDs were soldered in a straight line with arbitrary, but equal, spacing between each unit. Characterization tests show that this configuration did not provide a uniform distribution of light.

Based on a previous light intensity distribution study, an array was constructed that included a circle of LEDs with one unit located in the center as shown in Figure 4. The irradiance pattern model of this array predicts a smooth edge hexagon shape area of uniformity. For simplicity, we considered this shape to be a circle. Furthermore, intensity within 5% of the maximum intensity was set as the cutoff for the uniform area.

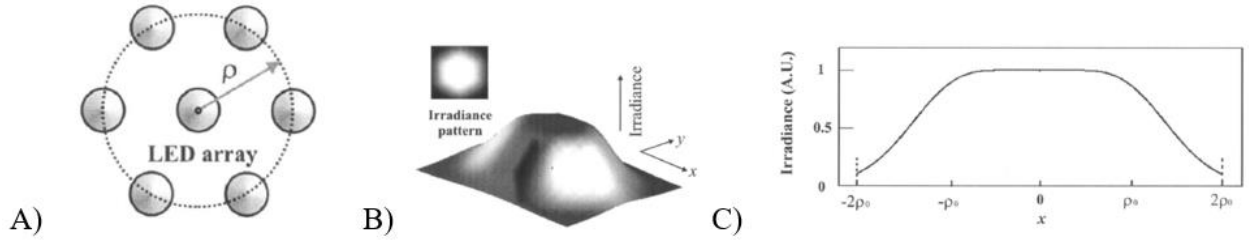

Figure 4. Circular geometry of the LED array with uniform area predictions. A) The physical arrangement of LEDs. B) 3D model of resulting irradiance pattern. C) Predicted normalized irradiance as a function of the displacement along any axis in the circle with ρ_0 representing the array's radius. (Figures provided courtesy of The Optical Society)

Equation (1) shows that the radius ρ_0 of the circle is dependent on a variable *m* and the height of the system *z*. The variable *m* takes into account the relative position of the LED emitting region from the curvature center of a spherical encapsulant. This constant depends on the value of the LED's half angle or viewing angle $\theta_{1/2}$, which is defined as the off-axis angle when irradiance is half of the maximum value. The Luxeon LED half angle values were found in their respective datasheets. The value of *m* can be calculated by equation (2) After considering the distance from the pyrex container's lid to the bottom of the PDMS sample, *z* was set to be about 2 – 2.5 in.

$$\rho_0 = \sqrt{\frac{4}{m+2} z} \tag{1}$$

$$m = \frac{-ln\,2}{ln(cos\theta_{1/2})} \tag{2}$$

Because each color of LED had a varied half-angle, the radii for their respective circles were marginally different. To avoid unwanted blockage of light, the LEDs were placed at a small distance laterally from each other. In summary, a circular LED array was designed with a radius calculated by considering parameters including the *m* variable, LED half angle, and height of source above the sample.

Circuit design

The electrical current that was required to power the 9 LED array was larger than the Arduino's 0.4 mA output limit, so a circuit needed to be designed to utilize an external power supply. Agilent's 3630 power supplies are common power supplies similar to others found in research labs and were used in our design. A MOSFET circuit was an easy way to use the Arduino to provide a low voltage signal to control the power supply.

Electrical characteristics and design factors of the LEDs were found in the manufacturer's specification sheet. For simplicity, the initial circuit was designed with the white LEDs, and then any needed adjustments were made for the colored LED arrays. Minimum and maximum operating voltages were determined to be 2.8 V and 3.4 V, respectively. Furthermore, the current required to make the LED emit at maximum intensity was approximately 200 mA. For 9 units, the total current was 2 A.

The MOSFET circuit had a configuration similar to the common-source amplifier where the LED load was connected to the drain, the gate was connected to the control signal, and the source was grounded. When selecting the optimal MOSFET for this project, 3 specifications needed consideration: Gate Threshold Voltage $V_{TH,}$ maximum Drain Current I_D, and the switching speed of the transistor. The V_{TH} needed to be relatively small to accommodate the low voltage control signal coming from an Arduino microcontroller. The transistor needed to be able to handle at least 2 A of drain current I_D to drive 9 LEDs. Additionally, switching speed of the transistor is fast enough to handle high-frequency I/O signals during experiments using low-time interval light cycles. The Vishay Siliconix IRF520 model MOSFET fit these requirements best.

During the design phase, OrCAD Capture simulation software was used to build and test the circuit before any physical prototyping or breadboarding. After contacting the LED and transistor manufacturers, SPICE models were retrieved for the LEDs and IRF520 transistor. Running a simulation to predict what diode currents one could expect for a range of gate voltages identified the linear range of control. This was done by simulating a DC voltage sweep across Arduino voltage [V10] as shown in Figure 5. Note that on each leg of the LED array's parallel connection, there is a single series resistor in place. When powering a parallel connection of LEDs with small internal resistances, it is necessary to consider the current variation that can result when the leg resistances vary. The current inconsistency caused the LEDs to shine at different intensities resulting in uniformity issues. For this reason, we included current balancing resistors on each leg of the parallel LED connection.

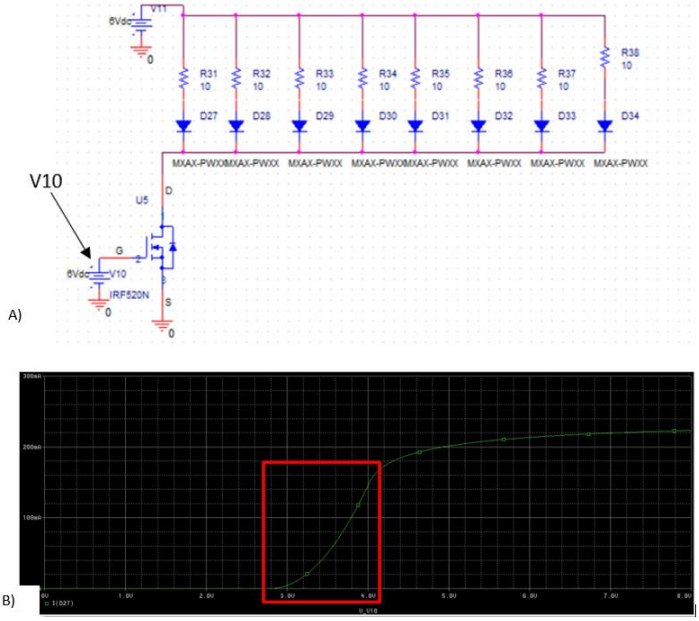

Figure 5. Schematic and resulting diode current-gate voltage characteristic plot for initial transistor simulation. A) Schematic used for sweeping DC voltages across the gate input [V10] of the IRF520 NMOS transistor. B) The resulting plot of diode current vs. gate voltage to find the linear region of control, as highlighted by the red box.

As seen in the simulation plot, the linear region falls between 2.8 V(V_0) and 4.1 V(V_f). After breadboarding and running this simulation with real components, V_f was found to actually be closer to 5.1 V

Arduino's analog PWM output pins provide 255 equally spaced steps from 0-5 V of the output voltage. To maximize the range in which linear control could be achieved, a Non-Inverting Summing Amplifier stage before the MOSFET was implemented. This operational amplifier (opAmp) circuit transformed the output of the Arduino's 0-5 V output to match the 2.8-5.1 V linear range by using a linear equation function. The transformation stage was connected to the input of the MOSFET, allowing the user to control the 0-5 V output of the Arduino for 255 equal steps of linear I_D control. This gives the user linear control of the intensity as a consequence. The operational amplifier was designed as shown in Figure 6.

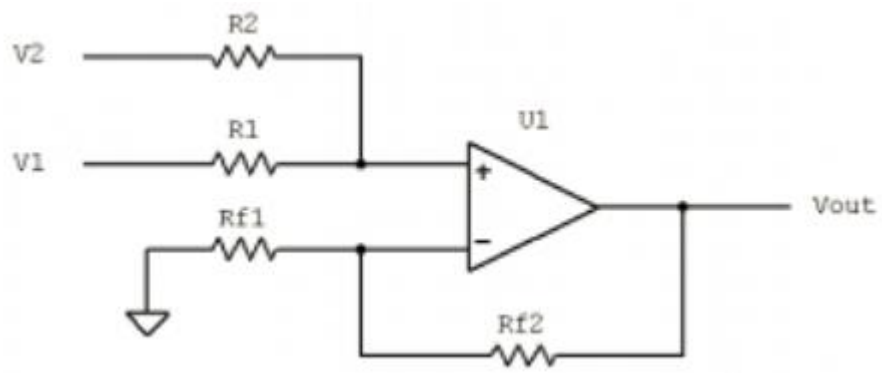

Figure 6. Non-Inverting Summing Amplifier configuration. Used to transform Arduino input voltage V1 into a suitable transistor input signal for linear I_D control.

$$Vout = \left(1 + \frac{Rf2}{Rf1}\right)\left(V1\frac{R2}{R1+R2} + V2\frac{R1}{R1+R2}\right) \quad (3)$$

Our amplifier integrated a linear function with two set conditions.

$$f(0) = V_{0,}\, f(5) = V_{f,}\, V_{out} = 0.46(V1) + 2.8 \quad (4)$$

Setting $\frac{Rf2}{Rf1} = 0$, and allowing V1 to be the Arduino input, the ratio of R1 & R2 and then V2 could be solved for. The solutions are as follows:

$$R1 = 1.174(R2)$$

$$V2 = 5.185$$

Using standard resistor values that were available, R1 and R2 were set to 38 kΩ and 33 kΩ, respectively. Rf2 was modeled as a wire, and Rf1 was set to a high resistance of 50 kΩ. As a result, $\frac{Rf2}{Rf1} = 0$.

With all circuit component values solved for, the circuit was built in OrCAD and simulated. The resulting plot in Figure 7 shows a linear relationship between the diode current and the gate voltage up to 2.75 V then saturates. This is explained by the ideal transistor model going beyond its linear operation region. In practice, this relationship will remain linear for the entire range of gate voltages supplied by the Arduino. A solution for gaining linear control over the drain current, and thus the LED intensity, was then achieved.

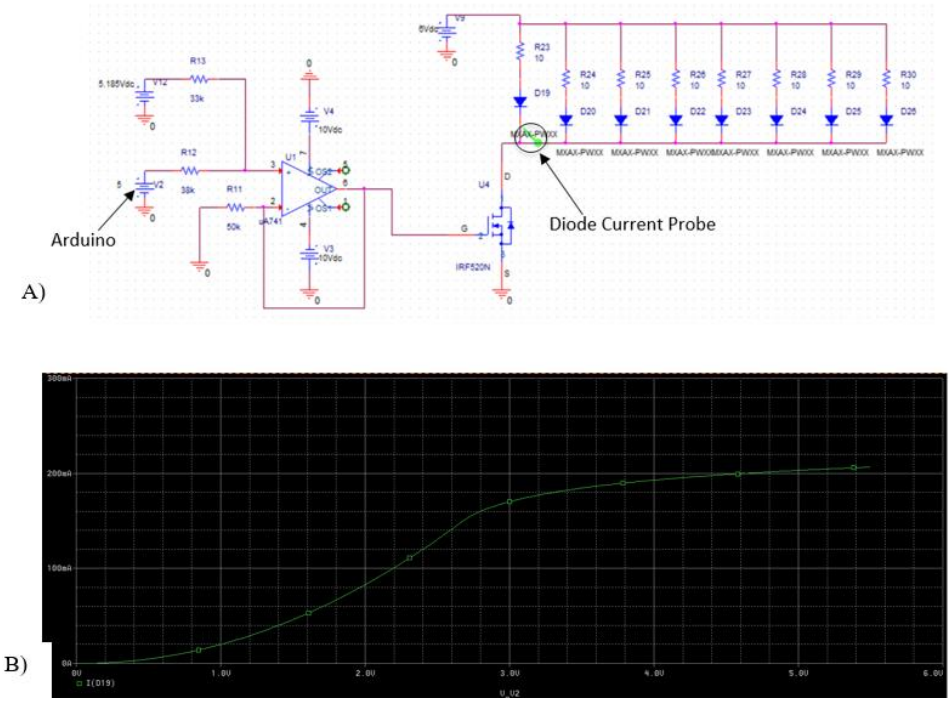

Figure 7. Complete circuit schematic and resulting current-gate voltage characteristic plot. A) Circuit with all components used to simulate and Arduino's 0-5 V with a DC sweep while measuring the current through one diode. B) Resulting plot of diode current vs. gate voltage.

Shown in the full circuit schematic, 4 voltage rails were used as a power source. On the standard Agilent 3630a power supply, there are only 3 voltage rails: providing up to 6 V and 2.5 A, +10 V and 0.5 A, and -10 V and 0.5 A, respectively. After concluding that the circuit required ±10 V rails for the saturation terminals on the opAmps, the power supply had one remaining high current 6 V rail that was used to drive the LED array. To accommodate the V2 voltage of 5.185 V, another power supply unit was needed. Considering that the opAmps require a minimal amount of current, V2 was jumped to the 6 V driving rail so that another power supply was not necessary, allowing the circuit to run on one standard power supply. After simulating with this adjustment, Figure 8 shows one minor tradeoff for this change. Seen in the simulation plot, the transistor was slightly turned on when the control signal is off. This translates to a loss of control over the low-end intensities. This is considered a fair tradeoff since we are not concerned with

experimenting at low intensities and used one less power supply than the previous design. Furthermore, additional control was gained over top-end intensities that are of interest.

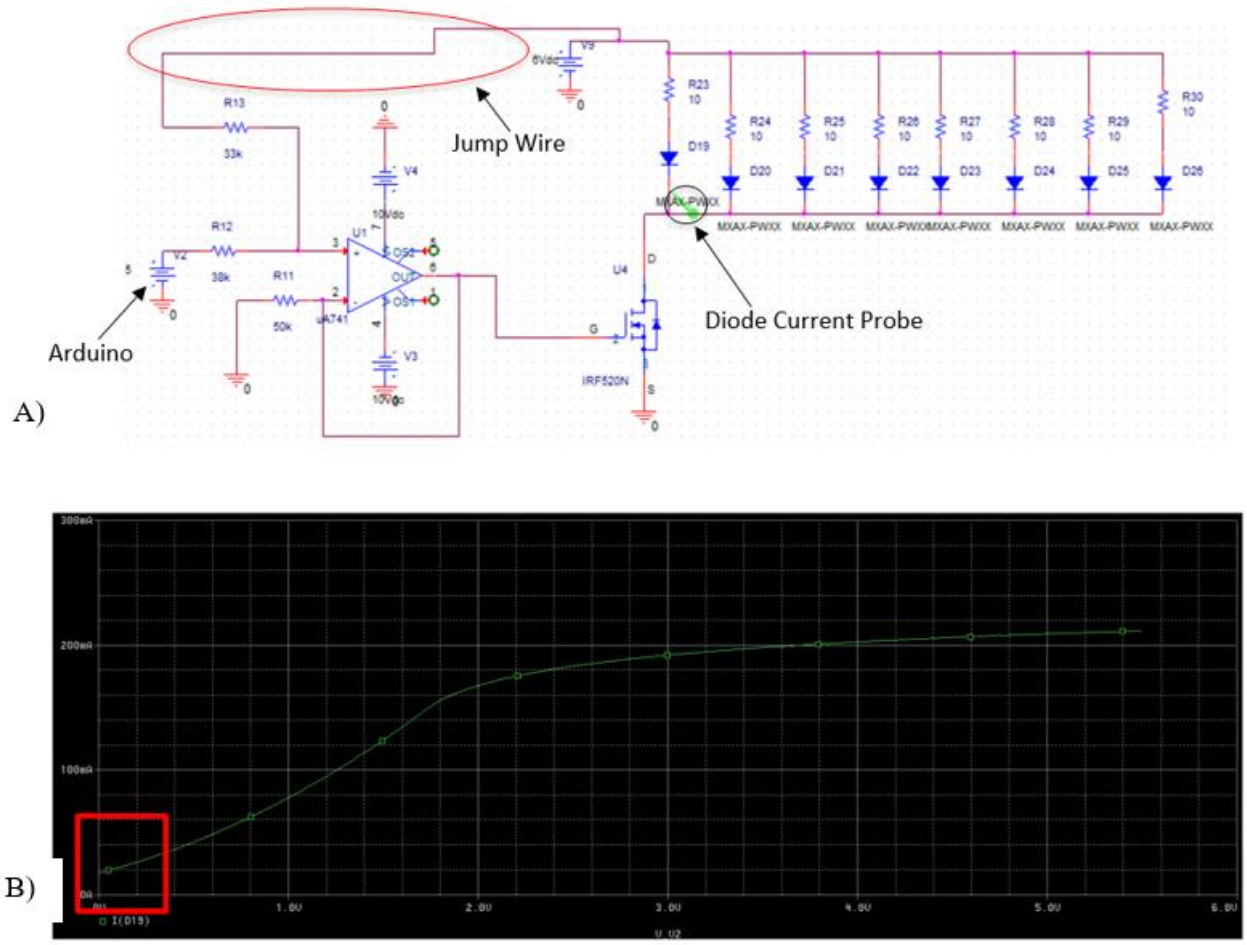

Figure 8. Final circuit schematic and resulting diode current-gate voltage characteristic plot. A) Circuit schematic with V2 jumped to the 6 V supply rail. B) Resulting characteristic plot showing a small current flowing at 0 V of gate voltage.

PCB fabrication

To accommodate the surface mount LED packages for trial runs of our circuit designs, fabricating PCBs was necessary. The Engineering Innovation Center EIC at Texas A&M University was utilized because it offered PCB design and fabrication support. Eagle Cadsoft was the software used to design, route, and generate Gerber files for the fabrication of the actual

PCB. Footprints are basic building blocks of every PCB circuit design that specify what will actually be printed on the board for a particular component. For example, our surface mount LEDs equated to two specially dimensioned contact pads on the board. Although Eagle offers libraries with similar package footprints as the LEDs we were using, it was more appropriate to manually create a footprint based on the datasheet specifications shown in Figure 9.

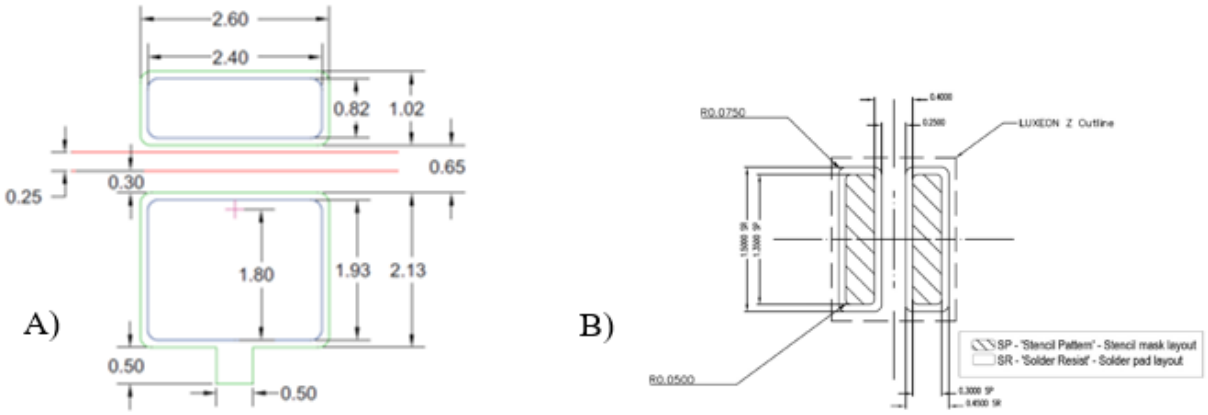

Figure 9. Solder Pad designs for the A) white and B) colored LEDs

Once the footprints were created, everything that was needed to build the circuit in Eagle's provided schematic editor had been completed. The EIC's PCB fabrication equipment had specific constraints for the dimensioning, spacing, and drilling that were considered when designing and routing the circuit for printing. The constraints included making traces that were not too narrow or close together, components were not placed too close to the edge of the board, and diameters of annular rings were not too small. While working within these constraints, some additional Eagle and Sparkfun libraries were used to enter the circuit into the schematic editor (Figure 10A). By default, Eagle transfers the circuit design to a PCB board view where one is able to manually place the components of a circuit on the board with precision. All of the

components apart from the LEDs were arranged to be as neat and out-of-the-way as possible to allow for the LED array to be isolated (Figure 10B). Eagle's autoroute function was partially used to fill up small width traces, but thicker traces that handle higher currents were manually routed. The EIC provided a file that Eagle could use during its auto routing to stay within the mentioned design constraints. After the circuit was designed, the prototypes were fabricated by soldering the surface mount LEDs on to the board by means of solder paste and a heat gun.

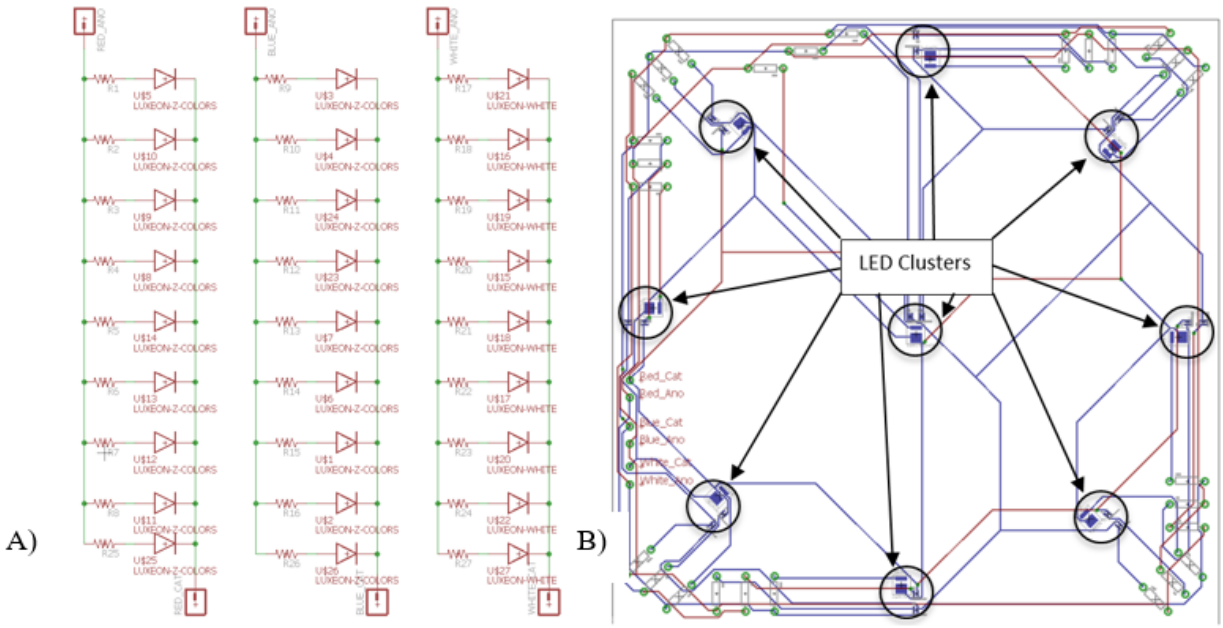

Figure 10. Eagle's PCB design interface. A) Full schematic of the LED array in schematic editor. B) Fully routed PCB board with clusters of LED footprints shown in the circular arrangement.

Light system characterization

The uniformity of light emitted from the circular array was then put to the test in a characterization setup. Important parameters to consider when constructing the characterization structure were the physical dimensions, the parallelism of the array to a light sensor, and an underlying grid to measure displacement. Figure 11 shows how the setup was constructed by using a PCB vise that was holding the LED array over a parallel surface marked with evenly

spaced gridlines. Placed on top of the flat gridded surface was a Li-Cor LI-190/R Quantum light sensor set to measure Photosynthetic Photon Flux (light intensity) in units of μmol photon s^{-1} m^{-2}. The height of the PCB vise was set to mimic the displacement between the pyrex container's lid and the microalgae samples in a microfluidic device. The array was centered upon a specified point on the grid by turning on the LEDs and then slowly moving the light sensor around to find the point of highest intensity. A quick check with the naked eye was used to confirm that the sensor did, indeed, look centered under the circular array. To measure the uniformity of the array, the sensor was moved away from the center 1 cm at a time and the corresponding intensity reading was recorded. This was done over a 5 to 7 cm radius. The uniformity was measured with white LEDs at different intensity setpoints.

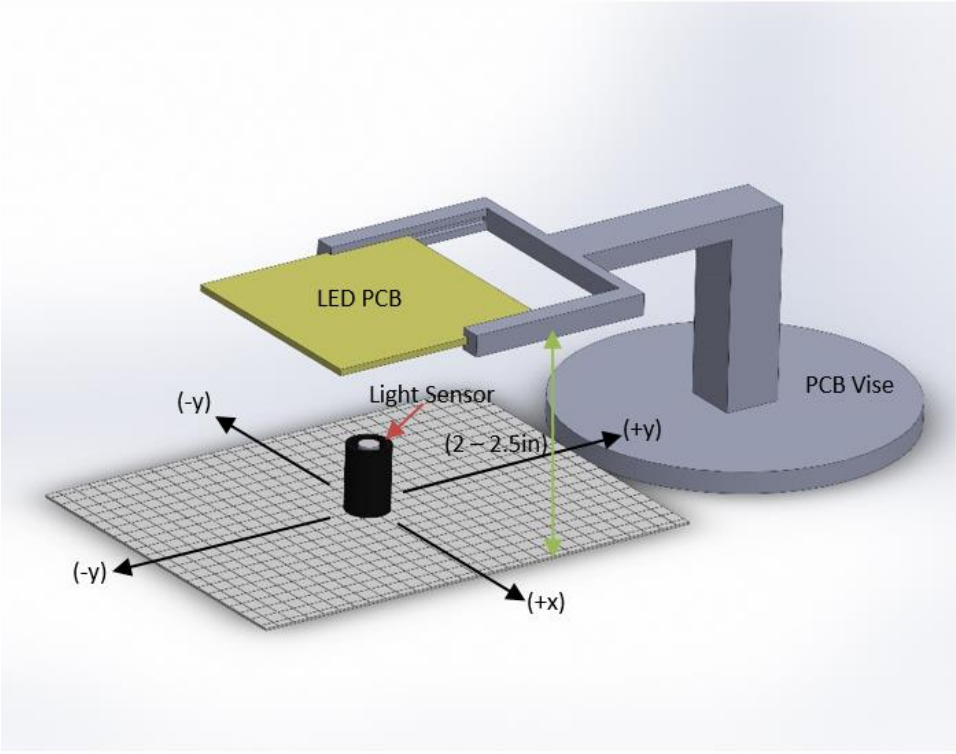

Figure 11. Characterization setup. The light sensor is placed on top of a grid while measuring intensities at different offsets from the center of the LED array. The LED array is soldered on a PCB that is held in place by a vise set to a specific height.

Figure 12 shows the relative light intensities measured at different displacements from the center using various intensity setpoints. Along the x-axis of the array, the intensity holds above 95% for 5 cm of displacement in the positive direction but suffers in the negative direction where the intensity dips below 95% at just 1.5 cm. Along the y-axis of the array, the intensity in the positive direction holds similarly to the negative x-direction, but the negative y-direction stays above 95% for about 3.5 cm. The circular array design was expected to give a uniform circular area with a radius approximately equal to the 5.7 cm radius of our array. The circular array constructed performed as described in the previous literature in 1 out of the 4 directions that were measured.

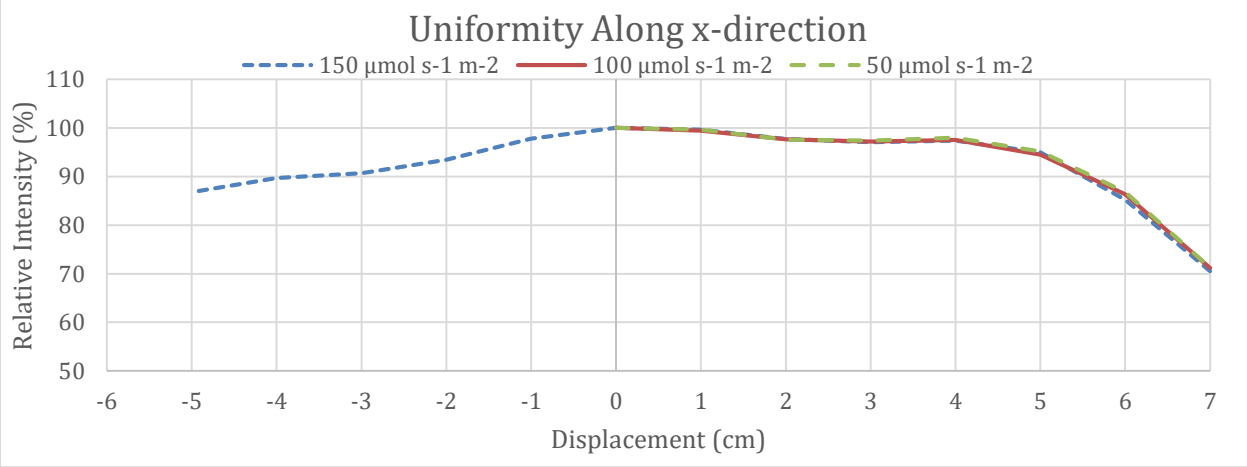

Figure 12. Uniformity along x-direction. Normalized light intensities at different displacements from the center (x=0).

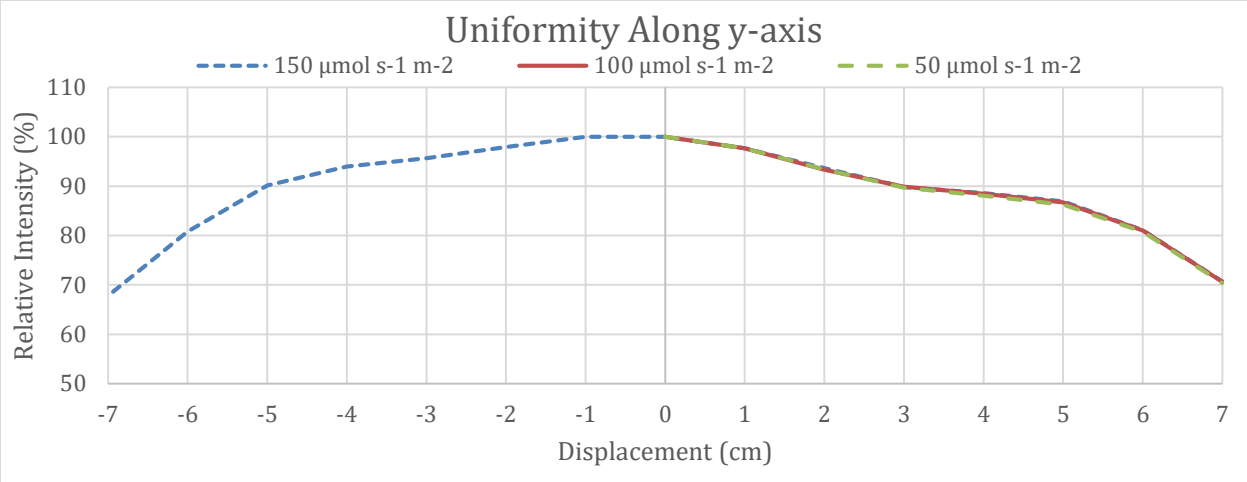

Figure 13. Uniformity along y-direction. Normalized light intensities at different displacements from the center (y = 0).

There are a few possible reasons for the results observed in the characterization. To find the center of the circular array, we assumed it was the point of greatest intensity. This method could lead to erroneous results because the point of highest intensity may not have actually been the center, shifting the graphs either left or right. Another possible cause for the non-uniformity observed in 3 of the measured directions was inconsistent intensities amongst the LEDs in the array. If the LEDs were shining at different intensities, the interference patterns used in the previous studies mathematical modeling were not as accurate, causing a non-uniform area of distributed light. Further tests were done to investigate the possibility of intensity variation amongst the LEDs in the array. Since the intensity of an LED depends on the amount of current flowing through it, the individual currents, resistances, and intensities were measured for each LED in an array. The individual intensities were measured by picking a constant arbitrary Arduino setting to supply one LED at a time with identical voltage and current and then measure its intensity from a set height. Using a digital multimeter, the resistances of and the currents through each LED were measured during operation. All of these tests were done at different arbitrary current/voltage setpoints. From the data in table 1, the variances in LED currents,

intrinsic resistances, and intensities obtained from their respective tests are shown. The resistances show a variation with a maximum difference of 1Ω, which was 8.8% of the maximum value measured. When measuring current through the individual LEDs, a considerable variation was observed with a maximum difference of 6.8 mA, which was 24.91% of the maximum value measured. During an individual LED intensity test, a marginal variation can be seen with a maximum difference of 6.55 μmol photon s^{-1} m^{-2}, which was 7.11% of the maximum value measured. These results suggest that although process variation during LED manufacturing may play a small role, the developed circuit design could be the cause for some variation in supplied currents to the LEDs.

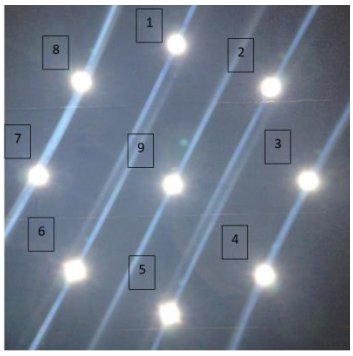

Figure 14. Numbered LED array. LEDs were assigned a number for comparison testing of individual currents, intensities, and intrinsic resistances.

Table 1. Measured LED characteristics.

A)

LED #	Current (mA)
1	27.3
2	24.5
3	24.1
4	24.8
5	25.3
6	24.4
7	20.5
8	22.5
9	26.7
Std Dev	2.05
Max delta	6.8
Detla %	24.91

B)

LED #	Measured LED resistance (Ω)
1	10.67
2	10.36
3	10.95
4	11.32
5	11.36
6	11.33
7	11.16
8	10.76
9	10.83
Std dev	0.35
Max delta	1
Delta %	8.80

C)

LED #	Intensity (μmol photon s-1 m-2)
1	88.84
2	85.67
3	89.23
4	87.01
5	92.15
6	89.17
7	85.6
8	89.62
9	91.64
Std dev	2.33
Max delta	6.55
Delta %	7.11

Overall, maximizing the area of uniform intensity is important for accommodating microfluidic testing platforms of various size. The positive x-direction uniformity measurement shows that with some adjustments to the circuit, the system has the potential to produce a circular uniform area of approximately 10 cm diameter. From the results, in the worst case, a circle of 3 cm diameter was a region of uniform distribution. As discussed, the serpentine microfluidic chambers used during our culture experiments were small enough to fit well within this area of light. For our experimentation purposes, this developed LED array provides a sufficiently large area of light.

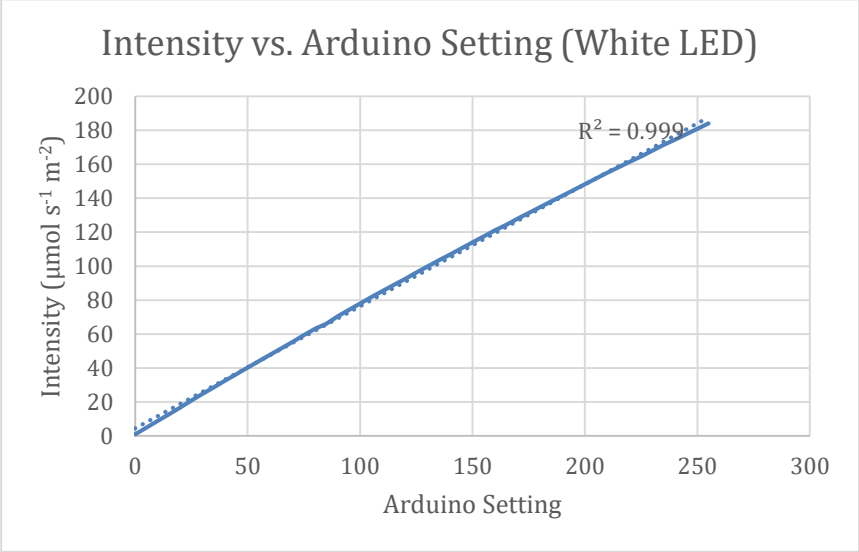

Figure 15. White LED intensity vs. Arduino setting. The plot shows the measured intensities for each Arduino setting during characterization and a linear relation between Intensity and Arduino setting.

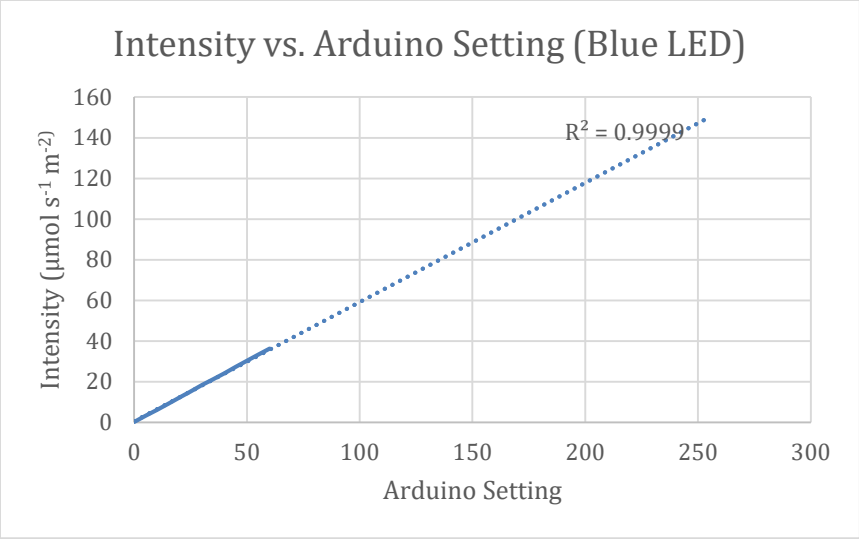

Figure 16. Blue LED intensity vs. Arduino setting. Plot showing the measured intensities for each Arduino setting during characterization. Shows linearity of the relationship between Intensity and Arduino setting.

Characterizing the control capabilities of the light system was done in a similar manner as the uniformity characterization. The range of intensities, linearity of control, and resolution of intensity steps were measured using the same PCB vise setup. With a stationary light sensor, the range of intensities was measured by sending control signals of values 0 and 255 to measure and record the low-end and top-end intensities, respectively. Linear control can be confirmed by measuring intensities at several Arduino control setpoints and plotting a graph of the data. Once linearity is confirmed, resolution of intensity control can be found by using the Intensity vs. Arduino Setting plot to determine how much intensity increases with every Arduino step. Figures 15 and 16 show intensity measurements plotted against the corresponding Arduino setting. A linear relationship is shown between the Arduino input control signal and the corresponding intensity measured, confirming the linear controllability of this system. Also shown on this plot are the achievable ranges for the white and blue colored LEDs: 0-185 µmol photon s^{-1} m^{-2} for white, 0-150 µmol photon s^{-1} m^{-2} for blue. The resolution for control was measured as 0.75 and 0.6 µmol photon s^{-1} m^{-2} per control step for the white and blue LEDs, respectively.

Culture experiment and results

To demonstrate the capabilities of the new LED subsystem in our overall PBR design, microalgae cell culture experiments were run to examine growth response under various light conditions. The first experiment had two culture setups where one was exposed to white light from the conventional incandescent light bulb and the other to white light from the array of 9 LEDs. Culture conditions such as temperature, light intensity, wavelength, light cycle, and nutrient concentration were kept constant at 21°C, 80 μmol photon s^{-1} m^{-2}, white (380 – 760 nm), and constant exposure (0ms) respectively. Figure 18 shows the growth response for the two different light sources. The start of exponential growth as well as the growth saturation points occurs on the same days for each culture. Additionally, the numbers of cells measured at saturation are similar between the two setups. The above observations indicate comparable performance between the conventional and developed light sources.

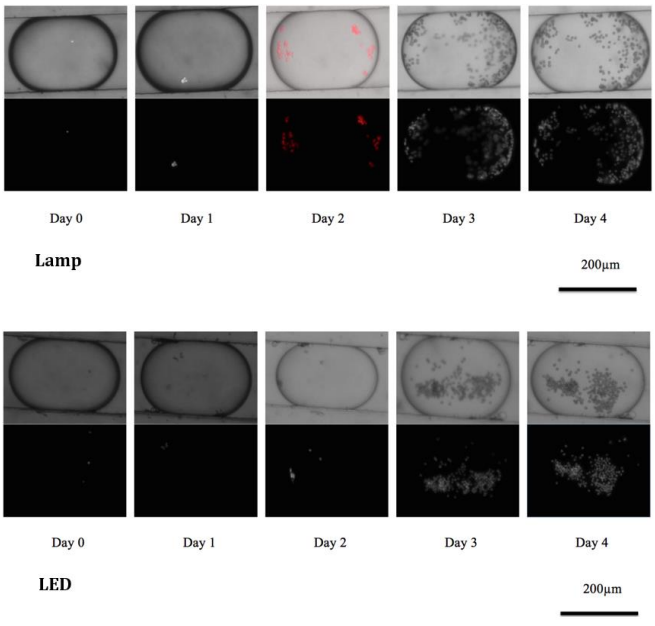

Figure 17. Brightfield and Autofluorescent images of microdroplets at under Lamp and LED light source. Microalgae was culture under the following conditions: 80 μmol photon m^{-2} s^{-1} intensity and 21˚C temperature. Droplets with one microalgal cell on day 0 were tracked over the course of 4 days.

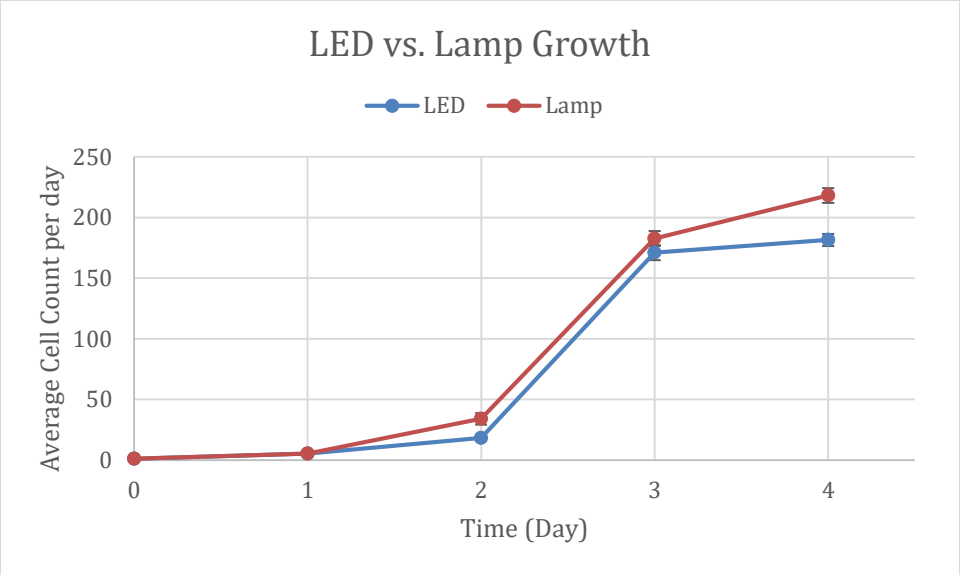

Figure 18. LED vs. Lamp culture experiment. Average cell count for 10 tracked droplets over a 5-day period for setups with and LED or Lamp light source.

An experiment was conducted where the wavelengths of light between two setups were modified while all other culture parameters were kept constant. The values were consistent with the Lamp vs. LED experiment. In this experiment, two LED setups were used: one shining white light (380 – 760 nm), one with blue light (450 – 495 nm). Figure 20 shows that under blue light, the microalgae exponential growth starts earlier than with white light exposure. Additionally, the saturation point of the blue light culture was considerably higher than that of the white light culture. [12] reported that the lowest specific growth rates were obtained by using blue LED in the photoautotrophic cultivation of Spirulina platensis. Furthermore, several studies reported that microalgae response to different wavelengths of light could vary by species [14]. These results and past studies could suggest that *C. reinhardtii* responds better to blue wavelengths of light than white.

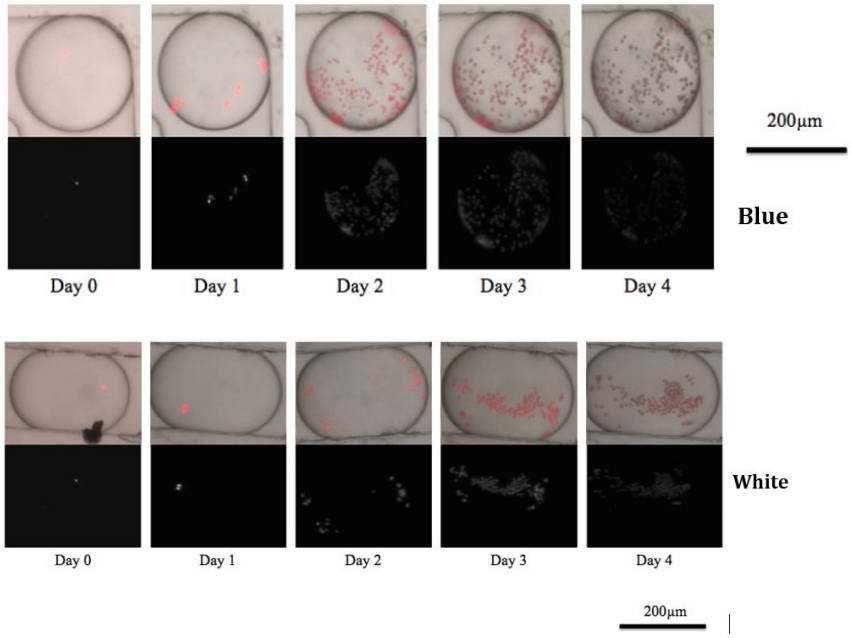

Figure 19. Brightfield and Autofluorescent images of microdroplets at under Blue and White LED light source. Microalgae was culture under the following conditions: 80 µmol photon m^{-2} s^{-1} intensity and 21˚C temperature. Droplets with one microalgal cell on day 0 were tracked over the course of 4 days.

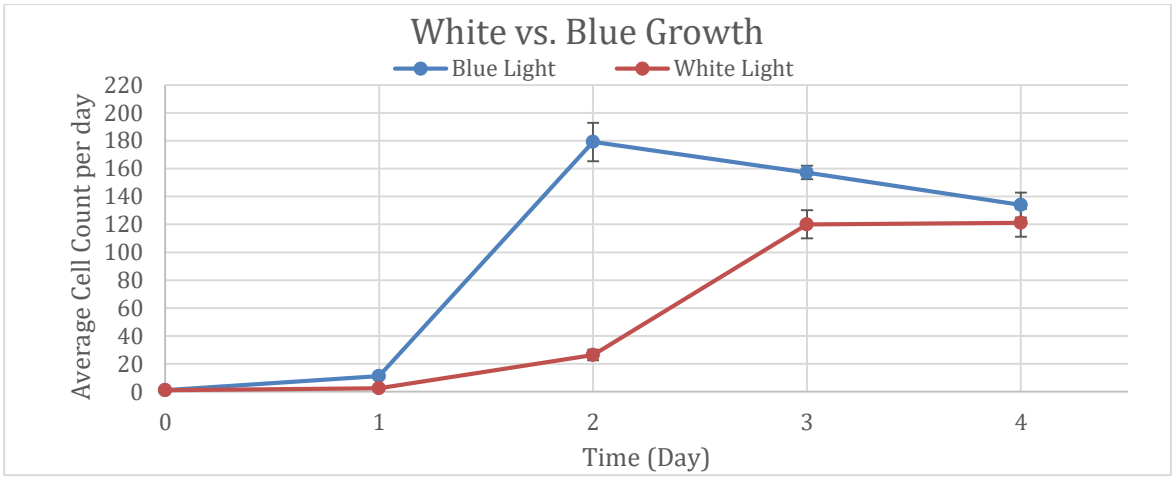

Figure 20. White vs. Blue culture experiment. Average cell count for 10 tracked droplets over a 4-day period for setups with a white (380 – 760 nm) or blue (440 – 460 nm) light source.

Another culture experiment investigated algae growth response to different intensities of white light. Culture conditions including temperature, wavelength, light cycle, and nutrient concentration were kept constant at the values mentioned in the above two experiments.

Furthermore, all light sources used in this experiment were the newly developed LED arrays. Figure 22 shows the growth rates for microalgae exposed to intensities ranging from 46 to 137 µmol photon s^{-1} m^{-2}. Exponential growth phases for the two higher intensities begin earlier than the lowest intensity. Also, the highest intensity has the steepest increase in cell count during its exponential growth. Lastly, the saturation point is highest for the greatest intensity culture but comparable for the two lower intensities. Our results suggest that the growth of *C. reinhardtii* is positively correlated with higher intensities during their growth phase, as also reported by other studies [15].

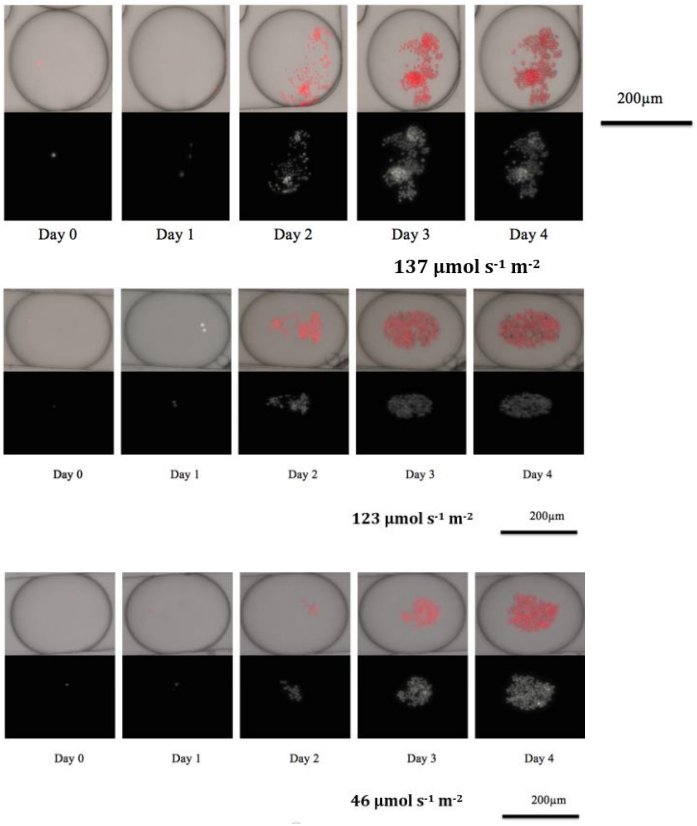

Figure 21. Brightfield and Autofluorescent images of microdroplets at under intensities ranging from 46 to 137 µmol photon s^{-1} m^{-2}. Microalgae was culture under the following conditions: white LED light and 21˚C temperature. Droplets with one microalgal cell on day 0 were tracked over the course of 4 days.

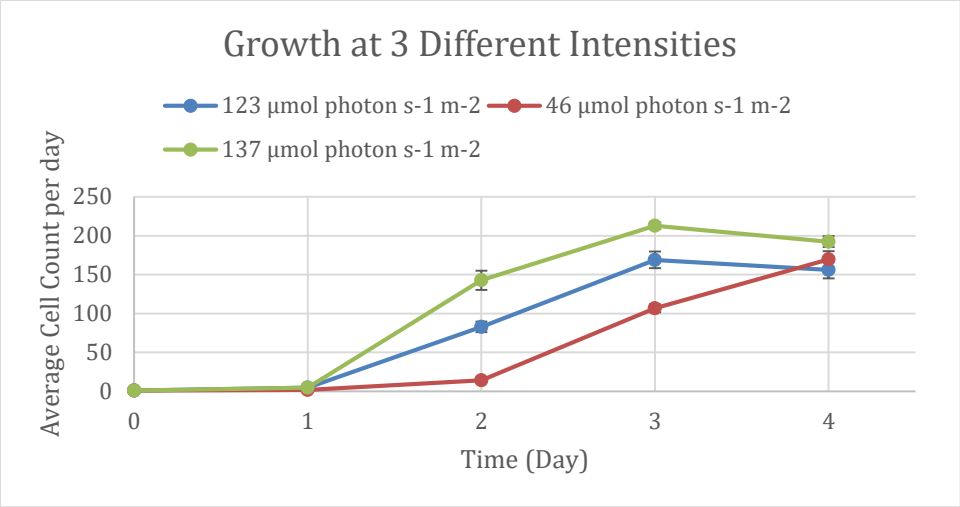

Figure 22. White vs. Blue culture experiment. Average cell count for 20 tracked droplets over a 4-day period for setups using light intensities ranging from 46 to 137 µmol photon s^{-1} m^{-2}.

CHAPTER IV

TEMPERATURE CONTROL SUBSYSTEM

Motivation for temperature control

Temperature effects the cellular chemical composition, uptake of nutrients and the growth rate of microalgae [16]. Temperature control is needed to study the effect of temperature on microalgal growth. The typical temperature range for optimal growth of most microalgal species is between 20-30°C [1]. Exposing microalgae to temperatures beyond this range can result in cell damage or death [2]. To accurately characterize microalgal oil and biomass yield, the temperature control subsystem was designed to maintain steady-state temperatures between room temperature (21°C) to 40°C.

The purpose of the temperature control subsystem is to produce a uniform temperature profile across a glass slide substrate bonded with a microfluidic device. This ensures all microalgal cells are exposed to a constant setpoint temperature. Being able to control a large area of uniform temperature will increase the testing throughput of the system by accommodating a large number of independent bioreactors.

Control system and circuit design

Proportional-integral-derivative (PID) feedback control mechanism is a popular algorithm used in control systems and is the basic principle of our temperature control module. A PID controller continuously calculates the error, e(t), between a set-point value and measured value. The controller aims to minimize this error over time by adjusting a control variable, y(t). The value of

the control variable is a weighted sum of three terms, namely proportional, integral, and derivative [17]. Mathematical model of the controller is as follows:

$$y(t) = K_P e(t) + K_I \int e(t)\, dt + K_D \frac{de(t)}{dt} \qquad (5)$$

The three constants: proportional K_P, integral K_I, and derivative K_D, are tuned for a specific system.

The temperature control system was designed using Proportional-Integral (PI) feedback control. A differential constant is important if a fast response is required from the system. Since most microalgal culture experiments extend over a course of 4 days, a PI controller was sufficient to reach stability.

First, a relay-based circuit was designed to implement the PI controller. An Arduino Uno microcontroller with a k-type thermocouple shield (Maxim MAX31855) was used to monitor the temperature of the heater. The thermocouple accuracy was ±0.25°C. If the measured temperature exceeded a set value, a relay attached to the heater disconnects the power supplied to the heater. Sunfounder's 2-channel 5 V relay shield module for Arduino Uno was selected for our design. A standard laboratory power supply at a voltage of 4 V was used to power the heater. The frequency at which the relay module turned on and off was determined by the output of the PI controller. This PI output was used as a control signal to regulate the magnitude and duration of current through the heater, which in turn regulated the temperature.

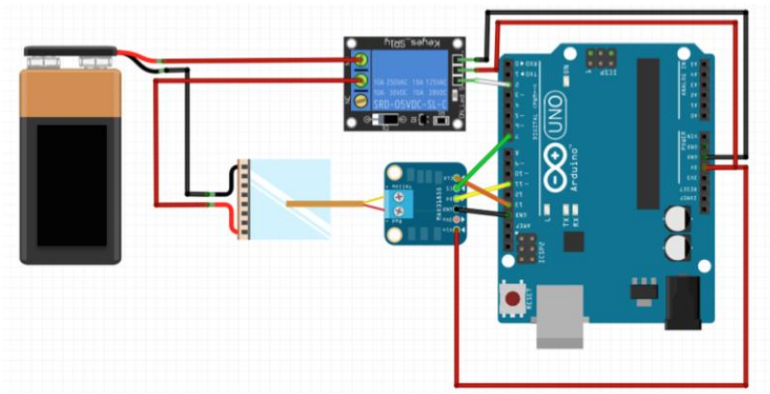

Figure 23. Circuit design for the temperature control system. An Arduino microcontroller was connected to a thermocouple shield and a relay. The relay was regulating the current through the heater

Next, the Arduino PID controller code was developed and manually tuned. All three PID constants were initially set to zero. The proportional constant K_P was increased until the output of the controller was stable, with a delta of less than 2%. The integral constant K_I was arbitrarily chosen, and adjusted until the minimum K_I value was found for which the output of the system was stable with less than 2% change. After controllability of one heater was achieved, the setup was expanded to include multiple heaters. This was done to observe the effect of implementing multiple PI controllers on the settling time of the setpoint temperature. The plot of PI output vs. time (Figure 24b) shows that we are able to achieve the setpoint temperature within 800 seconds since the start of the experiment even at higher temperature (34°C).

A)

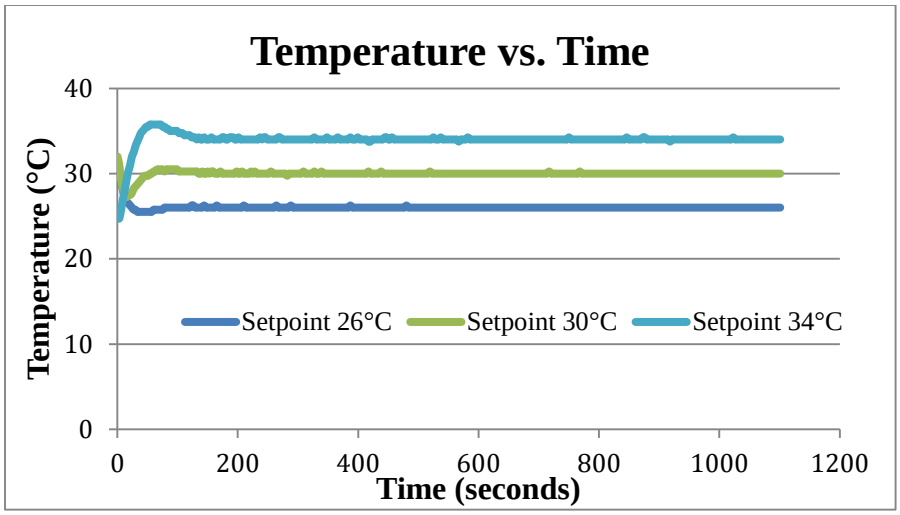

B)

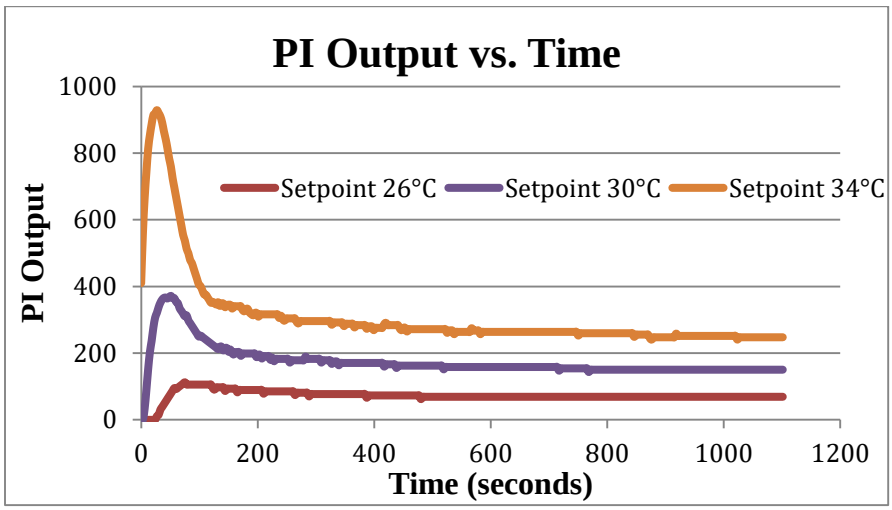

Figure 24. A) The plot of Reference Temperature versus Time. Measured temperature reference for the PI controller was recorded since the start of the experiment for multiple temperature setpoints. This was done to examine the effect of settling time at higher setpoint temperatures. B) The plot of PI output of the controller over time. The graph shows at even at higher setpoint temperatures, the system is able to stabilize within 800 seconds since the start of the experiment.

The two heating elements considered were Kapton heaters and Peltier thermoelectric cooling module. Kapton heaters are thin, flexible heaters sealed in a polyimide film. These heaters can achieve temperatures in the range -185°C to 200°C. Kapton heaters provide fast temperature response to changes in current. However, since these heaters are flexible, they need to be mounted on the glass slide each experimental setup with Kapton tape, with the possibility of

trapping air between the glass slide and heater. Kapton heaters unsuitable for this application due to inconvenient set-up and lack of close thermal contact between heater and glass slide.

Peltier thermoelectric cooling module from TE Technology Inc. was selected as the heating element for our final design. They are small, rigid, and lightweight with a temperature range of -40°C to 80°C. They offer temperature control with ±0.1°C accuracy. The rigid ceramic plate of the thermoelectric heaters makes them ideal for close thermal contact, maximizing efficiency of heat transfer. Their flat structure also simplifies the experimental set-up as the glass slide can rest on its surface. Furthermore, thermoelectric coolers offer rapid heat-up and cool down characteristics, allowing fast temperature control over short time intervals. The ability to heat and cool using the same module makes them ideal for extended future studies of microalgae below room temperature. We selected a 4.8 cm by 4.8 cm thermoelectric cooler due to the size closely matching the dimension of the glass slide (5 cm by 7.62 cm).

Thermal simulation

Obtaining an accurate steady state thermal profile of the surface between the glass slide and microfluidic device is needed to ensure that the temperature under the area of the microfluidic device is uniform. A uniform temperature distribution is needed for consistent culture temperature. Manual measurement of the temperature on this surface is impractical because the dimension of the k-type thermocouple is large compared to the device area resulting in low spatial resolution of manual measurements. Additionally, the surface is between the glass slide and bonded PDMS, so multiple thermocouples must be inserted into the PDMS during the fabrication process for measurements across the area of the device. COMSOL Multiphysics was used to simulate the thermal profile to simplify verification of temperature uniformity.

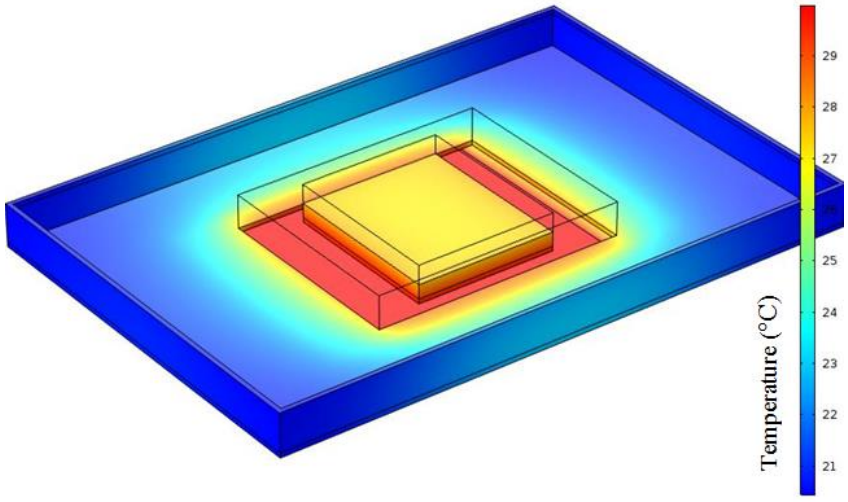

Figure 25. Simulation solution including the plastic dish, glass slide, PDMS device, and ceramic heater. The water, located inside the plastic dish above the microfluidic device, is hidden in this figure to show the device and glass slide underneath. The temperature profile shows that heat dissipates as the distance from the glass slide increases.

The model for the setpoint temperature profile on the surface of the heater was based on measured heater data (Figure 29). The simulated results were validated by the measured temperature on the surface of the glass slide by a thermocouple embedded in the microfluidic device. The simulation was built using the heat transfer in solids, heat transfer in fluids, temperature, and convective heat flux functions. The heat transfer coefficient was set to 5 W m^{-2} K^{-1} for the plastic/air interface and 20 W m^{-2} K^{-1} for the water/air interface. The results in Figure 26 were obtained using cut planes and cut lines. The resolution needed to model the uniformity characteristic was achieved by increasing the mesh resolution to extra fine. Five materials were used in the simulation: silica glass, PDMS, Acrylic plastic, water, and ceramic tuned to the heater's specifications. The simulation thermal solution confirms temperature uniformity on the glass slide under a 4 cm by 4 cm area of the microfluidic device.

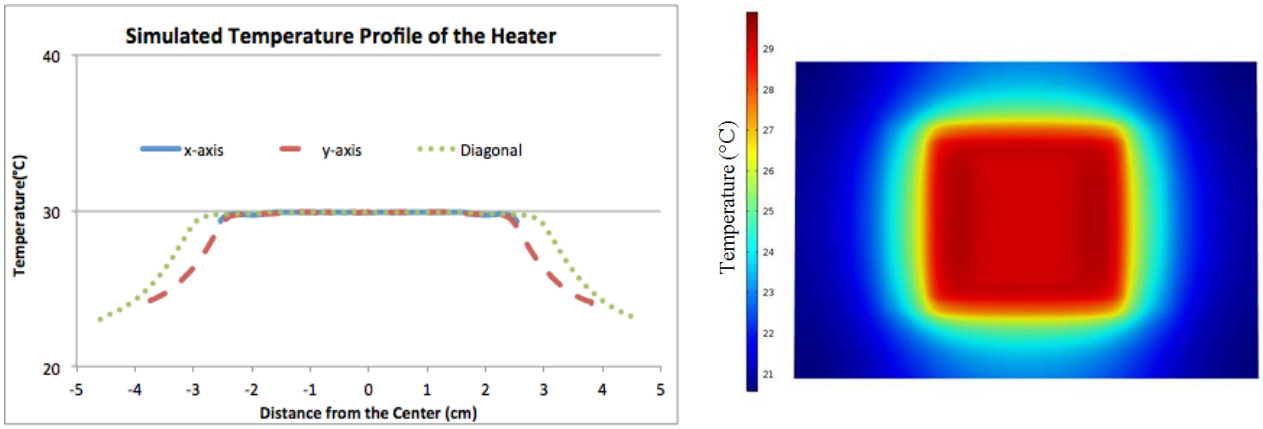

Figure 26. Analytical solution for temperature obtained from COMSOL. Initially the simulation included only the glass slide, microfluidic device, and heater to validate the analytical solution without the plastic water container. The simulation was then expanded to include liquid heat modeling.

Uniformity characterization results

To fully characterize our heat control subsystem, we needed to measure the temperature offset between the heater and the glass slide and the uniform area profile of the heater. The heater/glass offset was needed to account for the conduction losses in the system. The uniform area measurement was needed to identify the size of microfluidic devices compatible with our system. Uniform area was important for simulating the temperature profile along the glass slide.

Microalgal cells are placed in microfluidic channels directly in contact with the glass slide. Therefore, it is important to model the temperature offset between the heater and across the glass slide to know the actual temperature our microalgal sample is exposed to. First, to characterize the temperature offset, a microfluidic device was mounted on a standard 2” by 3” glass slide of 1mm thickness. The glass slide was secured to a petri dish, with a hole in its bottom, using Kapton tape. A thin layer of excess PDMS was used to seal the ends. The petri dish size is compatible with the microscope stage. The dish was filled with water at room temperature to mimic the actual experimental setup, as shown in Figure 27. The glass slide was then placed on a

4.8 cm by 4.8 cm thermoelectric heater. Thermocouple probes were mounted to the heater and embedded inside the PDMS substrate to study the effect of thermal conductivity between the heater and the glass slide at steady state. The temperature of a thermocouple attached to the heater was the reference for the PI controller. Thermal paste was applied at the point of contact of each thermocouple probe for improved heat conduction and accurate temperature measurements.

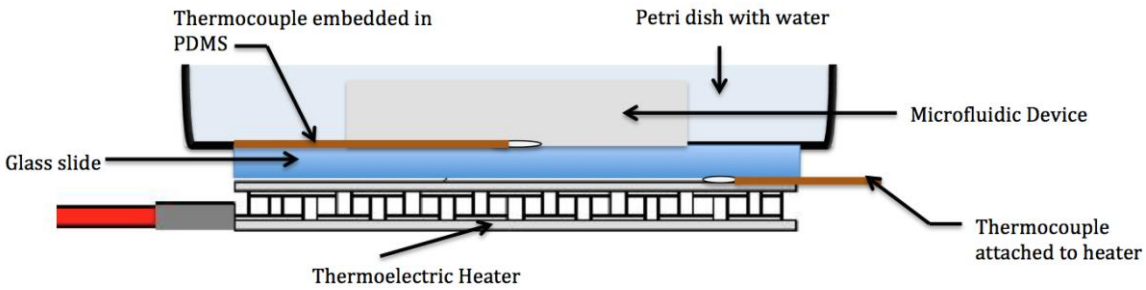

Figure 27. Characterization setup. The above setup was used to characterize the temperature offset between the heater and the glass slide. The thermocouple attached to the heater regulated the temperature through a PI controller. The temperature across the glass slide was recorded once the system reached steady state.

The relationship between heater setpoint temperature and measured microfluidic device temperature was modeled as shown in Figure 28. The setpoint temperature was varied between 25°C and 36°C. The system was left undisturbed for at least 2 hours before taking each reading; this was done to ensure the system had reached steady state. To achieve the desired temperature across the microfluidic platform, the heating element needed to be heated beyond the set temperature value to compensate for heat losses and lower thermal conductivity of glass. Conduction losses include the heat transferred to water, air and the remaining system. The graph Figure 28 shows that at higher temperatures, the offset between the heater and glass slide

increases. By modeling this offset into our system, we can account for the losses in the system and accurately control the temperature of microalgal culture.

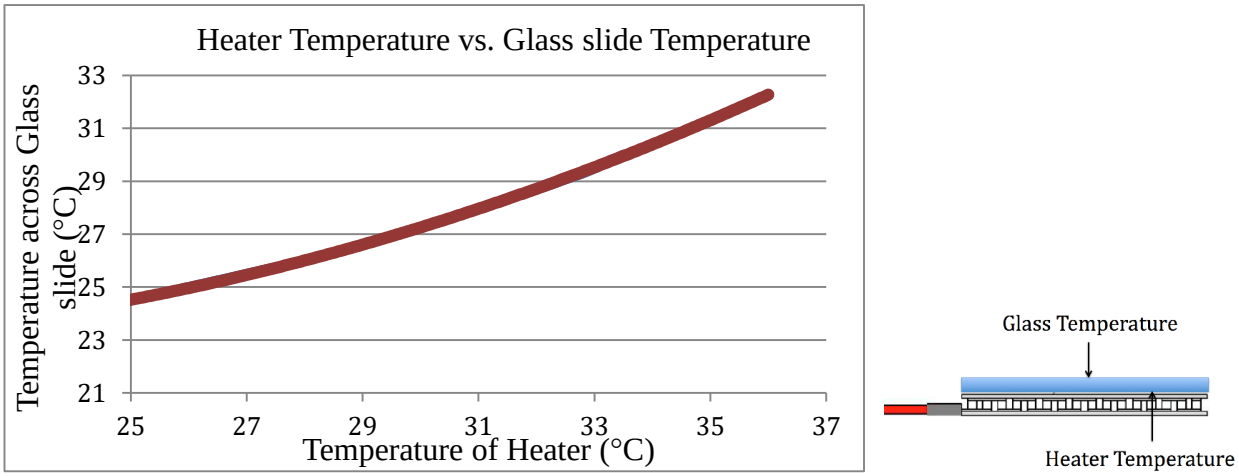

Figure 28. Graph of heater versus glass slide temperature. The offset between the heater temperature and the measured temperature across the thickness of the glass slide was recorded for several temperature setpoints.

Next, we measured the temperature profile of the 4.8 cm by 4.8 cm Peltier thermoelectric cooling module. It is important to achieve a large uniform area profile to ensure all microalgal cells are exposed to consistent temperature conditions for accurate culture experimentation. A thermocouple was secured in place at the center of the heater to implement PI control of the heater at a constant temperature (30°C). The heater was divided into four sections as shown in Figure 29, using a second thermocouple the temperature profile of the heater was measured along three directions x-axis, y-axis and diagonal. Readings were taken at 0.5 cm intervals along all three directions. The setup was allowed to reach steady state. Similar characterizations were done at different setpoint temperatures. Uniform temperature in an area of 4 cm by 4 cm was achieved with a maximum of 2% offset from the set-point temperature. Temperatures outside the 4 cm by 4 cm area were also found to be within 5% of the setpoint. Our system provides a uniform thermal profile for microfluidic devices that are within a 4 cm by 4 cm area.

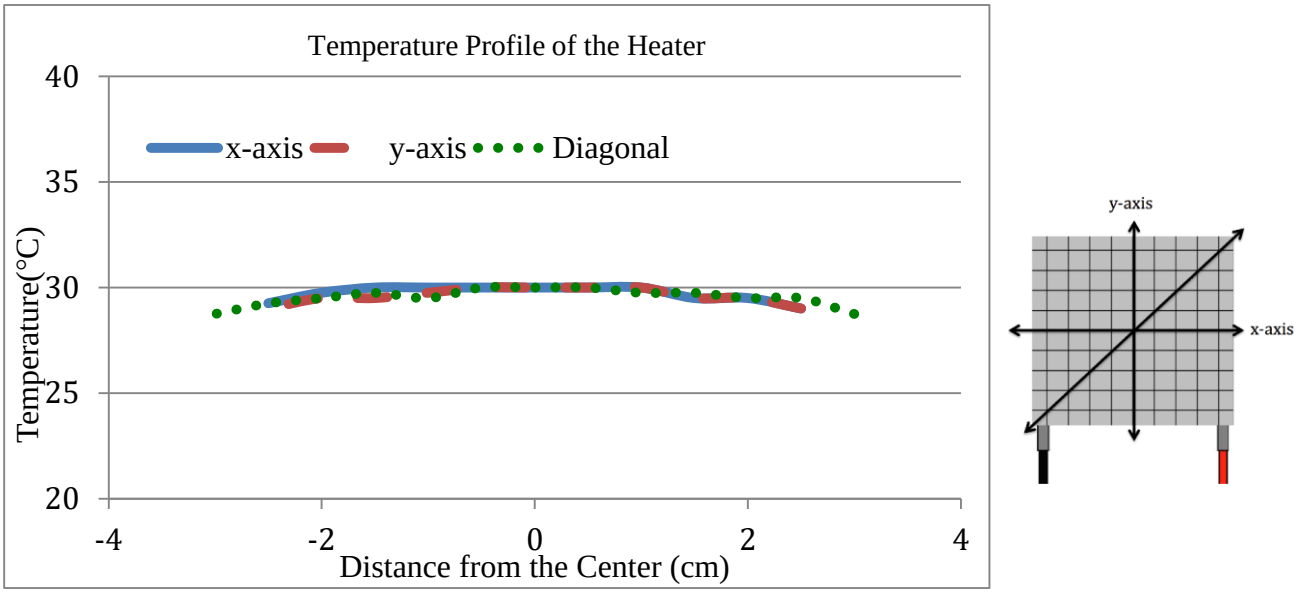

Figure 29. Temperature profile of the heater. A 4.8 cm by 4.8 cm Peltier thermoelectric cooling module was set at 30°C using a PI controller with reference temperature at the center. A second thermocouple was used to characterize the temperature across its area.

Culture experiment and results

To test the capabilities of our photo-bioreactor system, we performed cell culture experiments. Unicellular green alga *C. reinhardtii* were cultured at two uniform temperatures 26°C and 30°C. For an accurate comparison, all other conditions including light intensity, cycle, wavelength and nutrient concentrations were kept constant. White LEDs at a light intensity of 80 μmol photon m^{-2} s^{-1} were used. To avoid evaporation of droplets at a higher temperature, the microfluidic device needed to be immersed in water. Placing the heater under water can be an electrical hazard, therefore, we needed a design where the top half can be isolated from the bottom. A plastic tray with a 2" by 3" hole at its base was mounted on the glass slide, such that the slide was aligned with the base of the tray. Using Kapton tape the glass slide was held into place, a thin layer of excess PDMS was used to seal all four sides. The tray was filled with deionized water at room temperature to allow the system to reach steady state faster than using cold tap water.

Temperature readings were recorded throughout the experiment to ensure the setpoint temperature was maintained. Ten droplets were tracked per device at each temperature setpoint. Figure 32 shows the culture results for this experiment that suggests *C. reinhardtii* have a higher growth at 26°C as compared to 30°C. As the temperature is increased beyond the temperature for optimum protein synthesis growth rates are reduced [24].

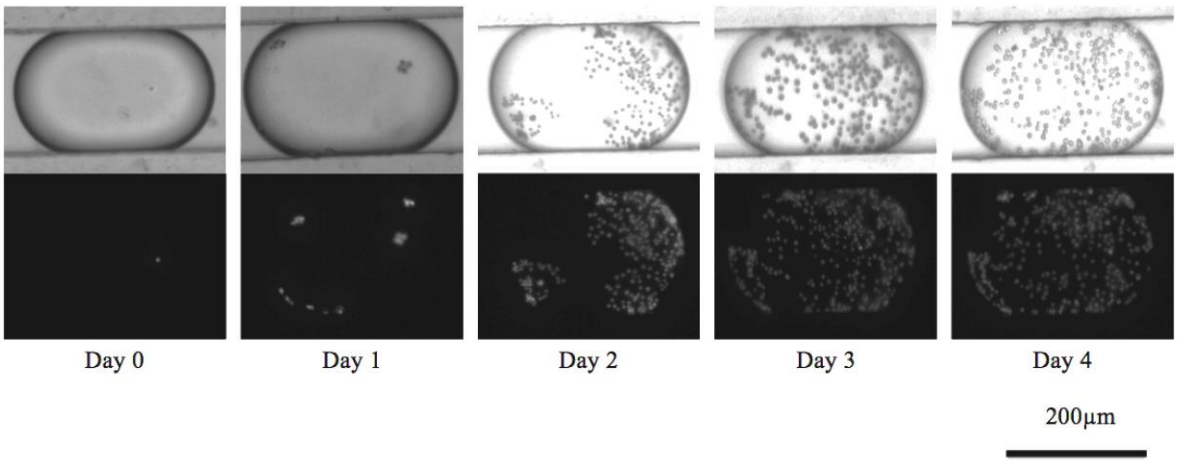

Figure 30. Brightfield and Autofluorescent images of microdroplets at 26˚C. Microalgae was culture under the following conditions: white LEDs at 80 µmol photon m^{-2} s^{-1} intensity and 26˚C temperature. Droplets with one microalgal cell on day 0 were tracked over the course of 4 days.

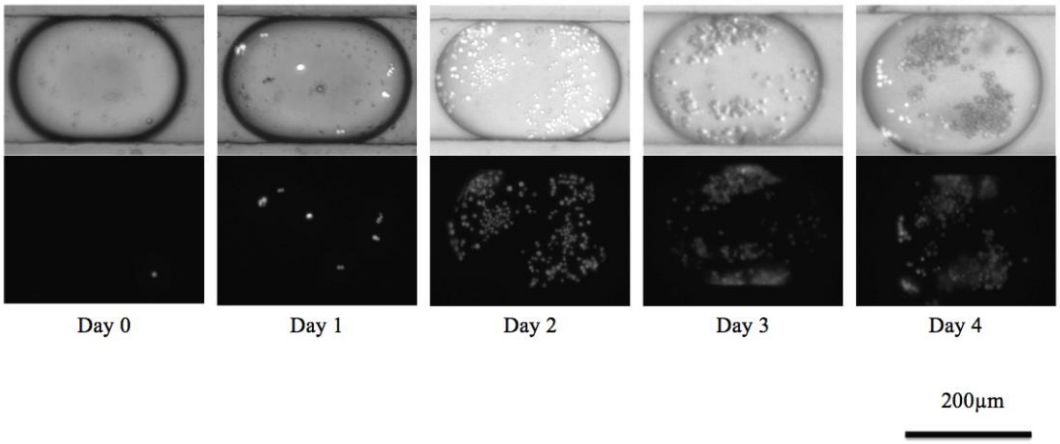

Figure 31. Brightfield and Autofluorescent images of microdroplets at 30˚C. Microalgae was culture under the following conditions: white LEDs at 80 µmol photon m^{-2} s^{-1} intensity and 30˚C temperature. Droplets with one microalgal cell on day one were tracked over the course of 4 days.

By day 4 the size of droplets at 30°C was observed to be slightly smaller as compared to 26°C as shown in Figure 30 and 31, respectively. A possible reason for this is that the rate of evaporation is higher at 30°C. Also, an air bubble was observed in the channel, which could increase the pressure in the channel causing the droplet to shrink.

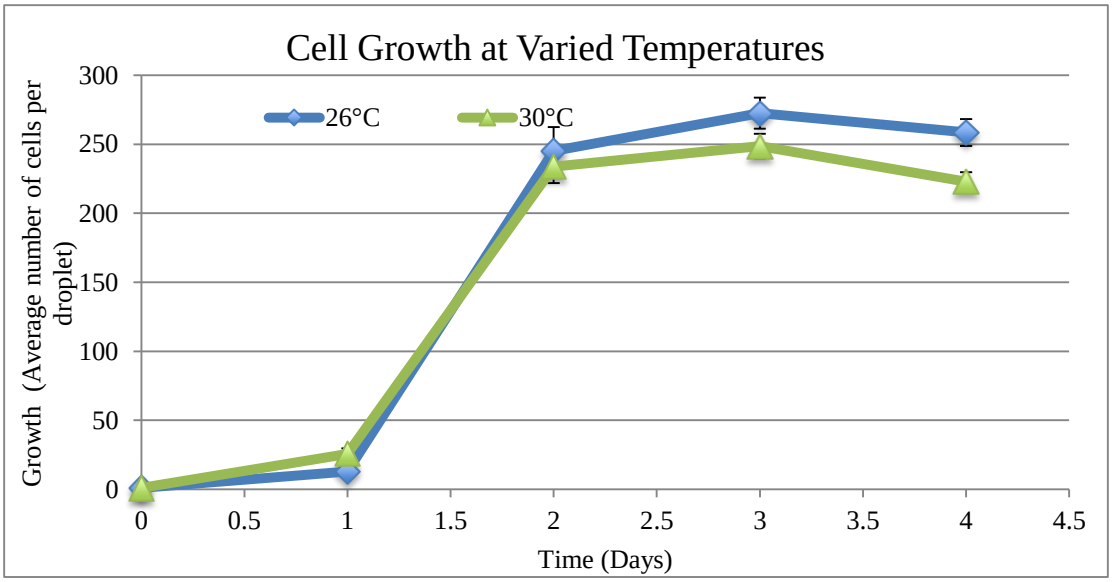

Figure 32. Cell growth at varied temperatures. Culture experiment results comparing the growth of *C. reinhardtii* at two temperatures 26°C and 30°C, respectively. The growth was measured by counting the average number of microalgal cells in a droplet per day. Data shows the average growth seen in 10 droplets at each temperature.

In summary, the relationship between setpoint temperature and measured microfluidic device temperature was used to model thermal losses to ensure accurate temperature control. The steady-state accuracy of the combined control system is ±0.25°C. Additionally, the system can achieve uniform heat profile in a 4 cm by 4 cm area with a 2% offset from the setpoint temperature. The temperature control system has been built, and the above culture results show its potential for use in microalgal growth characterization experiments.

CHAPTER V

CONCLUSION AND FUTURE DIRECTION

Conclusion

An inexpensive system to control growth conditions of cultures on a microfluidic device has been constructed. Temperature control reaches steady-state temperature uniformity under the area of channels in a microfluidic screening platform. The PBR's controlled LED light source is able to vary light intensity and wavelength in a circular uniform area over a culture platform. The microfluidic, temperature, and light systems were integrated into a PBR setup.

The PBR accommodates any microfluidic device design that is within the temperature and light area constraints listed in Table 2. Compared to a bulky lamp system, the PBR is compact and easier to setup, enhancing the user's ability to quickly iterate microfluidic experiments. Our culture results validate the potential of the PBR in experiments to optimize culture conditions of microalgae.

Future direction

By producing a temperature gradient across a microfluidic chip, testing throughput can be increased by changing temperature conditions between droplets. The temperature control subsystem can be extended to produce a linear temperature gradient by mounting multiple thermoelectric cooler modules along a single glass slide. Each of the heater modules can be set to a different temperature setpoint such that the overall all heat profile shows a linear temperature gradient. We simulated this design consideration using COMSOL Multiphysics resulting in the

solution shown in Figure 33. Additionally, the temperature dependent culture experiments can be extended to include temperatures below room temperature (21°C) in order to study their effect on the growth of *C. reinhardtii*.

Table 2. Photobioreactor System Characteristics.

Light Intensity	White LEDs 0 -185 μmol photon s^{-1} m^{-2} with a resolution of 0.75 μmol photon s^{-1} m^{-2} per control step
	Blue LEDs 0-150 μmol photon s^{-1} m^{-2} with a resolution of 0.60 μmol photon s^{-1} m^{-2} per control step
Wavelength Options	White (380-760 nm)
	Blue (450-470 nm)
Uniform Area of Light	3 cm diameter circle
Temperature Range	21℃ to 35℃
Uniform Area of Temperature	4 cm x 4 cm
Steady-State Accuracy of Temperature	±0.25℃

The next step in the development of the light system is the characterization of red LEDs. In the future, the system can be extended to include linear light intensity gradient to change light exposure between droplets on the microfluidic device. Culture experiments that combine various capabilities of the system such as light cycles, intensities, wavelength and temperatures can be performed to further the characterization of optimal microalgal growth conditions.

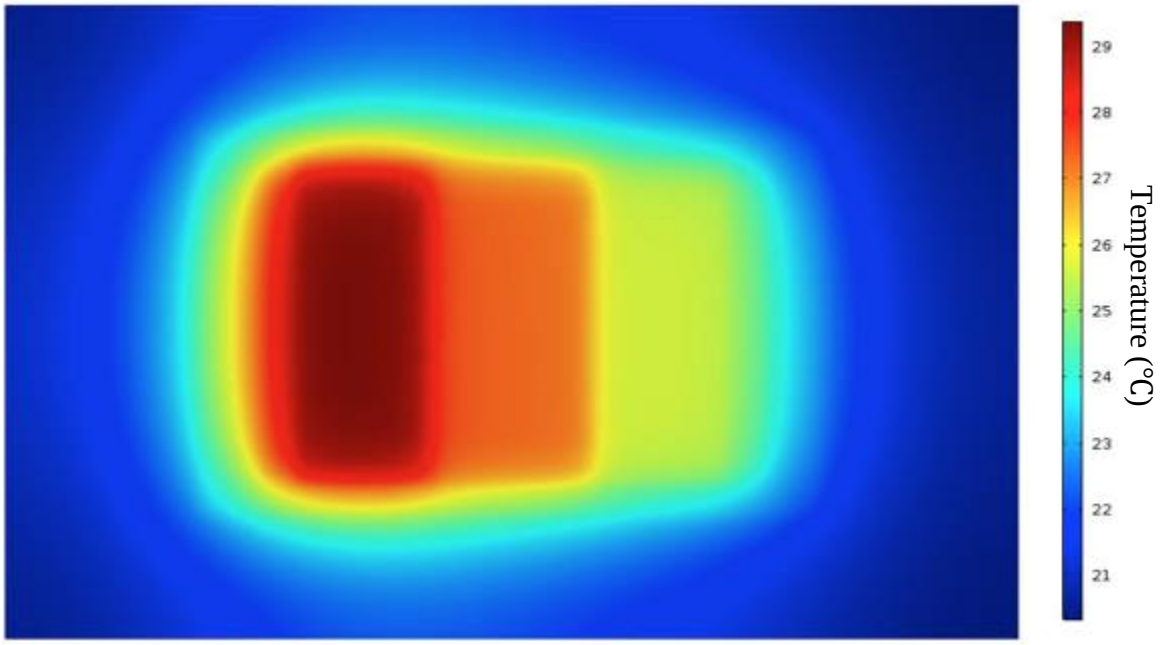

Figure 33. The thermal profile of a linear temperature gradient design.

REFERENCES

[1] D. R. Georgianna and S. P. Mayfield, “Exploiting diversity and synthetic biology for the production of algal biofuels,” *Nature*, vol. 488, no. 7411, pp. 329–335, Aug. 2012.

[2] T. M. Mata, A. A. Martins, and N. S. Caetano, “Microalgae for biodiesel production and other applications: A review,” *Renew. Sustain. Energy Rev.*, vol. 14, no. 1, pp. 217–232, Jan. 2010.

[3] Y. Chisti, “Biodiesel from microalgae,” *Biotechnol. Adv.*, vol. 25, no. 3, pp. 294–306, 2007.

[4] T. M. Squires and S. R. Quake, “Microfluidics: Fluid physics at the nanoliter scale,” *Rev. Mod. Phys.*, vol. 77, no. 3, pp. 977–1026, Oct. 2005.

[5] G. M. Whitesides, “The origins and the future of microfluidics,” *Nature*, vol. 442, no. 7101, pp. 368–373, Jul. 2006.

[6] D. Mark, S. Haeberle, G. Roth, F. von Stetten, and R. Zengerle, “Microfluidic lab-on-a-chip platforms: requirements, characteristics and applications,” *Chem. Soc. Rev.*, vol. 39, no. 3, p. 1153, 2010.

[7] A. Piruska, I. Nikcevic, S. H. Lee, C. Ahn, W. R. Heineman, P. A. Limbach, and C. J. Seliskar, “The autofluorescence of plastic materials and chips measured under laser irradiation,” *Lab. Chip*, vol. 5, no. 12, pp. 1348–1354, Dec. 2005.

[8] D. Bodas and C. Khan-Malek, “Hydrophilization and hydrophobic recovery of PDMS by oxygen plasma and chemical treatment—An SEM investigation,” *Sens. Actuators B Chem.*, vol. 123, no. 1, pp. 368–373, Apr. 2007.

[9] C. Barahona and E. Rigoberto, “Development of a microfluidic, segmented-flow, single molecule, enzyme activity assay and improvement of separation efficiency of basic proteins by application of a water- proofing agent as a coating in capillary electrophoresis,” Aug. 2012.

[10] S. Bae, C. W. Kim, J. S. Choi, J.-W. Yang, and T. S. Seo, “An integrated microfluidic device for the high-throughput screening of microalgal cell culture conditions that induce high growth rate and lipid content,” *Anal. Bioanal. Chem.*, vol. 405, no. 29, pp. 9365–9374, Oct. 2013.

[11] T. Glawdel, C. Elbuken, and C. L. Ren, “Droplet formation in microfluidic T-junction generators operating in the transitional regime. I. Experimental observations,” *Phys. Rev. E*, vol. 85, no. 1, p. 016322, Jan. 2012.

[12] C.-Y. Wang, C.-C. Fu, and Y.-C. Liu, “Effects of using light-emitting diodes on the cultivation of Spirulina platensis,” *Biochem. Eng. J.*, vol. 37, no. 1, pp. 21–25, Oct. 2007.

[13] E. Sforza, D. Simionato, G. M. Giacometti, A. Bertucco, and T. Morosinotto, “Adjusted Light and Dark Cycles Can Optimize Photosynthetic Efficiency in Algae Growing in Photobioreactors,” *PLoS ONE*, vol. 7, no. 6, p. e38975, Jun. 2012.

[14] C.-Y. Chen, K.-L. Yeh, R. Aisyah, D.-J. Lee, and J.-S. Chang, “Cultivation, photobioreactor design and harvesting of microalgae for biodiesel production: A critical review,” *Bioresour. Technol.*, vol. 102, no. 1, pp. 71–81, Jan. 2011.

[15] C. C. Ribeiro, J. Choi, L. Fung, and O. Kushniryk, “Effect of varying light intensity on cell abundance of Chlamydomonas reinhardtii,” *The Expedition*, vol. 2, 2013.

[16] S. P. Singh and P. Singh, “Effect of temperature and light on the growth of algae species: A review,” *Renew. Sustain. Energy Rev.*, vol. 50, pp. 431–444, Oct. 2015.

[17] Chengming Lee and Rongshun Chen, “Optimal Self-Tuning PID Controller Based on Low Power Consumption for a Server Fan Cooling System,” *Sens. 14248220*, vol. 15, no. 5, pp. 11685–11700, May 2015.

[18] Y. Chisti, “Biodiesel from microalgae beats bioethanol,” *Trends Biotechnol.*, vol. 26, no. 3, pp. 126–131, 2008.

[19] H. S. Kim, T. L. Weiss, H. R. Thapa, T. P. Devarenne, and A. Han, “A microfluidic photobioreactor array demonstrating high-throughput screening for microalgal oil production,” *Lab. Chip*, vol. 14, no. 8, p. 1415, 2014.

[20] N. R. Moheimani, “The culture of coccolithophorid algae for carbon dioxide bioremediation,” Murdoch University, 2005.

[21] D. Mark, S. Haeberle, G. Roth, F. von Stetten, and R. Zengerle, “Microfluidic lab-on-a-chip platforms: requirements, characteristics and applications,” *Chem. Soc. Rev.*, vol. 39, no. 3, p. 1153, 2010.

[22] P. Fairley, “Introduction: Next generation biofuels,” *Nature*, vol. 474, no. 7352, pp. S2–S5, Jun. 2011.

[23] S.-Y. Teh, R. Lin, L.-H. Hung, and A. P. Lee, “Droplet microfluidics,” *Lab. Chip*, vol. 8, no. 2, p. 198, 2008.

[24] A. Konopka and T. D. Brock, “Effect of Temperature on Blue-Green Algae (Cyanobacteria) in Lake Mendota,” *Appl. Environ. Microbiol.*, vol. 36, no. 4, pp. 572–576, Oct. 1978.

[25] A. Fatona, Y. Chen, M. Reid, M. A. Brook, and J. M. Moran-Mirabal, “One-step in-mould modification of PDMS surfaces and its application in the fabrication of self-driven microfluidic channels,” *Lab Chip*, vol. 15, no. 22, pp. 4322–4330, 2015.

[26] A. Piruska, I. Nikcevic, S. H. Lee, C. Ahn, W. R. Heineman, P. A. Limbach, and C. J. Seliskar, “The autofluorescence of plastic materials and chips measured under laser irradiation,” *Lab. Chip*, vol. 5, no. 12, pp. 1348–1354, Dec. 2005.

[27] T. Glawdel, C. Elbuken, and C. L. Ren, “Droplet formation in microfluidic T-junction generators operating in the transitional regime. I. Experimental observations,” *Phys. Rev. E*, vol. 85, no. 1, p. 016322, Jan. 2012.